UHRF1 drives the poor prognosis associated with RB loss in osteosarcoma

Stephanie C. Wu[1,2], Jocelyne Lopez[1], Kelsey Salcido[1], Loredana Zocchi[2], Jie Wu[3,4], and Claudia A. Benavente[1,2,4]

[1]Department of Developmental and Cell Biology, University of California, Irvine, CA 92697, USA.

[2]Department of Pharmaceutical Sciences, University of California, Irvine, CA 92697, USA.

[3]Department of Biological Chemistry, University of California, Irvine, CA 92697, USA.

[4]Chao Family Comprehensive Cancer Center, University of California, Irvine, CA 92697, USA.

Correspondence:

Claudia A. Benavente

University of California, Irvine

839 Medical Sciences Ct, Sprague Hall 108

Irvine, CA 92697, USA

Phone: 949-824-7845

E-mail: Claudia.benavente@uci.edu

ABSTRACT

Loss of function mutations at the retinoblastoma (*RB1*) gene are associated with increased mortality, metastasis and poor therapeutic outcome in several cancers, including osteosarcoma. However, the mechanism(s) through which *RB1* loss worsens clinical outcome remain to be elucidated. Ubiquitin-like with PHD and Ring Finger domains 1 (UHRF1) has been identified as a critical downstream effector of the RB/E2F signaling pathway that is overexpressed in various cancers. Here, we show that UHRF1 upregulation is critical in rendering osteosarcoma cells more aggressive. We confirmed that UHRF1 is transcriptionally regulated by the RB/E2F pathway and overexpressed in osteosarcoma. Using novel genetically engineered mouse models, we determined that *Uhrf1* loss dramatically reverses the effects of *Rb1* loss. Based on gain- and loss-of-function assays, we report that UHRF1 promotes cell proliferation, migration, invasion, and metastasis. Furthermore, transcriptome analyses revealed the involvement of urokinase-type plasminogen activator (uPA) in UHRF1-mediated cell mobility. Our work presents a new mechanistic insight into *RB1* loss-associated poor prognosis, revealing UHRF1 as a critical driver of tumor promotion, progression, and metastasis in osteosarcoma. This study provides substantial support for targeting UHRF1 or its downstream effectors as novel therapeutic options to improve current treatment for osteosarcoma and other cancers with RB/E2F pathway inactivation.

37 **INTRODUCTION**

38

39 Sarcomas are defined as malignancies that arise in tissues derived from the embryonic mesoderm such
40 as bone, cartilage, fat, muscle and the vascular system [1]. Among various kinds of sarcomas,
41 osteosarcoma (OS) is the most common primary cancer of bone and typically occurs in children and
42 young adults. As a highly metastatic cancer, 15-20% of osteosarcoma patients are diagnosed after the
43 cancer has already metastasized (typically to the lungs), which translates to 5-year survival rates of <40%
44 [2]. In comparison, patients without metastases have survival rates of 65-75%. Unfortunately,
45 pulmonary metastases occur in nearly half of all osteosarcoma patients [3]. OS survival rates have
46 plateaued since the introduction of adjuvant and neoadjuvant multiagent chemotherapy in the early
47 1980s [4]. The current treatment paradigm includes generic chemotherapeutic agents such as
48 methotrexate, cisplatin, and doxorubicin. Thus, there is a pressing clinical need to determine the factors
49 responsible for metastasis in osteosarcoma to facilitate development of new therapeutic strategies.

50

51 The most common genetic mutations found in OS are in tumor suppressors *TP53* and *RB1* [5, 6]. Loss-of-
52 function mutations of the *RB1* gene in OS are associated with poor therapeutic outcome as defined by
53 increased mortality, metastasis, and poor response to chemotherapy [7-11]. However, the mechanism(s)
54 through which RB loss leads to poor prognosis remains to be elucidated. RB has been implicated in
55 regulating most major epigenetic processes, including DNA methylation, histone modifications, and
56 microRNA regulation [12-16]. A previous study in retinoblastoma identified Ubiquitin-like, containing
57 PHD and RING finger domains 1 (UHRF1) as a key target gene downstream of the RB/E2F signaling
58 pathway that is abnormally upregulated following the loss of RB, and contributes to tumorigenesis [17].
59 UHRF1 is a multi-domain protein that exerts various functions that include, but are not limited to,
60 reading and writing of epigenetic codes, thus having the potential to significantly impact epigenome

upon deregulation. UHRF1 is most known for its role in maintaining DNA methylation throughout replication by recruiting DNA methyltransferase 1 (DNMT1) to hemi-methylated DNA at the replication fork. In recent years, many reports have emerged having observed the overexpression of UHRF1 in different types of human cancers including lung, breast, bladder, colorectal cancer, and retinoblastoma [17-21]. Thus, we hypothesized that loss of RB in OS contributes to tumor progression and increased malignancy through deregulation of its downstream target UHRF1.

In this study, we identified UHRF1 as a key player in OS tumorigenesis, promoting proliferation, migration, and metastasis. One of the most promising results was the induction of invasiveness by UHRF1 overexpression mediated by the urokinase-type plasminogen activator (uPA). Inhibition of uPA with a small-molecule inhibitor caused a robust decrease in OS migration and invasion. Loss of *Uhrf1* in developmental OS mouse models drastically delayed tumor onset, decreased pulmonary metastasis, and increased the life span of mice carrying *Rb1* mutations. These findings highlight the critical role of *Uhrf1* as a driver of the poor prognosis associated with RB loss and presents UHRF1 and its downstream targets as a novel therapeutic targets for OS.

MATERIALS AND METHODS

Xenografts, mouse models and cell lines

The five orthotopic xenografts used in this study: SJOS001105 (PDX1), SJOS001112 (PDX2), SJOS001107 (PDX3), SJSO010930 (PDX4), and SJOS001121 (PDX5) were obtained from the Childhood Solid Tumor Network [22]. Athymic nude (NU/J) mice were obtained from The Jackson Laboratories. The *p53*^{lox} and *Rb1*^{lox} conditional-knockout mice were obtained from the Mouse Models of Human Cancer Consortium at the National Cancer Institute; the *Osx-cre* mice were obtained from The Jackson Laboratory. The

85 *Uhrf1*-conditional knockout mouse was generated from mice obtained from the European Mouse
86 Mutant Archive, backcrossed to flipasse (Flp) mice for removal of the neo-cassette (tm1c conversion),
87 and then backcrossed to C57BL/6N mice for Flp removal. Mice were monitored weekly for signs of OS.
88 Moribund status was defined as the point when tumors had reached 10% body weight or induced
89 paralysis in the mouse. The University of California Irvine Institutional Animal Care and Use Committee
90 approved all animal procedures.
91
92 OS cell lines 143B, SJSA-1, SaOS-2 and U-2 OS, as well as MSCs and HEK293T cells were acquired from
93 ATCC. 143B were cultured in MEM (Gibco), with 10% BCS, penicillin/streptomycin, and 0.015mg/ml BrdU.
94 SJSA-1 were cultured in RPMI (Gibco), with 10% BCS and penicillin/streptomycin. SaOS-2 were cultured
95 in McCoy's 5A (Gibco), with 10% BCS and penicillin/streptomycin. U-2 OS were cultured in McCoy's 5A
96 (Gibco), with 15% BCS and penicillin/streptomycin. MSCs were cultured in Alpha-MEM (Gibco), with 10%
97 FBS and penicillin/streptomycin, HEK293T cells were culture in high-glucose DMEM (Gibco), with 10%
98 BCS, penicillin/streptomycin and sodium pyruvate. Cells were passaged every 3 to 4 days or when they
99 reached 70-80% confluence. At the time of passage, cells were split to 20% confluence.
100
101 **FDG-PET/microCT scan**
102 Mice were fasted overnight. Mice were injected with 0.1-0.5 mCi of ^{18}F-FDG in sterile saline (~ 0.05 to
103 0.2 ml) intraperitoneally (i.p.) and allow to uptake the ^{18}F-FDG for 60 min prior to imaging. Animals were
104 anesthetized and laid in supine position on the scanner holder with continued anesthesia. Scanning data
105 was acquired in full list mode and sorted into a single frame, 3 dimensional sinogram, which was
106 rebinned using a Fourier rebinning algorithm. The images were reconstructed using 2-dimensional filter
107 back projection using a Hanning Filter with a Nyquist cut off at 0.5 and corrected for attenuation using
108 the Co-57 attenuation scan data. Analysis of PET was conducted using PMOD 3.0 and IRW software. The

109 PET data was co-registered to the CT template for drawing regions-of-interest (ROI). The ROI data was
110 converted to standard uptake value (SUV) of ^{18}F-FDG.
111
112 **Western blotting**
113 Cell pellets or tumor tissues were homogenized by pipetting or pellet pestle in RIPA buffer (50 mM Tris-
114 HCl, pH=8, 150 mM NaCl, 1% NP-40, 0.5 % Sodium deoxycholate, 0.1% SDS, 1 mM EDTA) supplemented
115 with protease inhibitor (cOmplete™, Mini, EDTA-free Protease Inhibitor Cocktail, Roche). Samples were
116 allowed to lyse for 30 min on ice before centrifugation at 14000 RPM at 4° for 30 min. Protein
117 concentration was measured using BCA protein assay (Pierce™ BCA Protein Assay Kit). 40µg of total
118 protein were resolved in 4-15% SDS-PAGE gel (Mini-PROTEAN TGX Gels (4-15%), Bio-rad), and
119 transferred onto PVDF membrane (Immobilon-P Membrane, PVDF, EMD Millipore) using semi-dry
120 transfer apparatus (Bio-rad). Ponceau S stain was used to validate successful transfer. Non-specific
121 binding was prevented by incubating the membrane in 3% non-fat dry milk in TBS-0.25% Tween (TBS-T)
122 for 1 hour at room temperature, shaking. Primary antibodies were diluted in 0.5% non-fat dry milk in
123 TBS-T as follows: 1:1000 anti-Uhrf1 (sc-373750, Santa Cruz Biotechnology), 1:1000 anti-Rb (9313T, Cell
124 Signaling). Membranes were incubated in primary antibody overnight, shaking, at 4°C. Membranes were
125 then rinsed 3 times with TBS-T on shaker and incubated with secondary antibody for 40min at room
126 temperature, shaking. Secondary antibodies were diluted in 0.5% non-fat dry milk in TBS-T as follows:
127 1:1000 peroxidase labeled anti-mouse IgG (PI-2000, Vector Laboratories), 1:1000 peroxidase labeled
128 anti-rabbit IgG (PI-1000, Vector Laboratories). Membranes were again rinsed 3 times with TBS-T on
129 shaker. Chemiluminescence were detected using SuperSignal™ West Pico Chemiluminescent Substrate
130 (34077, Thermo Scientific). Relative band intensities were analyzed using ImageJ software.
131
132 ***In situ* hybridization**

133 Osteosarcoma tissue microarrays, containing 40 cases of osteosarcoma, duplicate cores per case, were
134 purchased from US Biomax, Inc (OS804c). 6 stage IA (T1N0M0), 16 stage IB (T2N0M0), 1 stage IIA
135 (T1N0M0), 16 stage IIB (T2N0M0) and 1 stage IVB (T2N1M0) tumors are represented in the array. Stage I
136 tumors are low grade and stage II and IV are high grade. The extent of the primary tumor (T) is classified
137 as intercompartmental (T1) or extracompartmental (T2). Tumors that have metastasized to nearby
138 lymph nodes are denoted by N1, but no distant organ metastases (M0) are represented in the array.
139 Formalin-fixed, paraffin-embedded (FFPE) slides were incubated at 60°C for 1hr for deparaffinization,
140 followed by two washes of xylene and two washes of 100% ethanol for dehydration, 5min each at RT,
141 before air-drying. RNAscope® technology was utilized for *in situ* hybridization. Assay was performed
142 following manufacturer's protocol. Human and mouse UHRF1-specific probes were customized by Bio-
143 Techne. RNAscope® Positive Control Probe- Hs-PPIB/Mm-PP1B and RNAscope® Negative Control Probe-
144 DapB were used. OpalTM 570 fluorophore was used at a 1:1000 dilution. Slides were mounted with
145 ProLong Gold Antifade Mountant.
146
147 **Chromatin immunoprecipitation (ChIP assay)**
148 ChIP assays were performed as previously described [23]. ChIP DNA was analyzed by qPCR with SYBR
149 Green (Bio-Rad) in ABI-7500 (Applied Biosystems) using the following primers. For motif 1 (M1), Forward:
150 5'-CCACATTCCCTCGCAGTATTTA-3'; Reverse 5'-CCCTGAACTCTTAAGTCCAAGTC-3'; for motifs 2 and 3 (M2,
151 M3), Forward: 5'-CACCCTCTTTCTCGCTTCC-3'; Reverse 5'-TGCCAGCTGCTCTGATTT-3'. The anti-E2F1
152 (3742; Cell Signaling) and rabbit IgG (sc-2027, Santa Cruz Biotechnologies) antibodies were used.
153
154 **Real-time RT-PCR (qPCR)**
155 Total RNA was isolated from cells or tumor tissues by homogenizing samples with TRIzol Reagent. RNA
156 was isolated through chloroform extraction. 1 µg of total RNA was used for cDNA synthesis with the

157 SuperScript™III First-strand synthesis system (Invitrogen) according to manufacturer's protocol at a
158 reaction volume of 20 µl. Quantitative PCR amplification was performed using 1 µl of reverse-
159 transcribed product in Power SYBR Green PCR Master Mix (4367659, Life Technologies). Primers were
160 designed using IDT Real-Time PCR tool (Integrated DNA Technologies). Reaction was carried out using
161 7500 Real-Time PCR system (Applied Biosciences). Data were normalized to those obtained with
162 endogenous control 18S mRNA and analyzed using ΔΔCt method. Primer sequence for PCR amplification
163 are as follows: UHRF1 (sense: 5'-GCTGTTGATGTTTCTGGTGTC-3'; antisense: 5'-
164 TGCTGTCAGGAAGATGCTTG-3'), PLAU (sense: 5'-GAGCAGAGACACTAACGACTTC-3'; antisense: 5'-
165 CTCACACTTACACTCACAGCC-3'), SEMA3E (sense: 5'- CTGGCTCGAGACCCTTACTG-3' ; antisense: 5'-
166 CAAAGCATCCCCAACAAACT-3'), HAS2 (sense: 5'-TCCATGTTTTGACGTTTGCAG-3'; antisense: 5'-
167 AGCAGTGATATGTCTCCTTTGG-3'), LAMC2 (sense: 5'-CACCATACTCCTTGCTTCCTG-3'; antisense: 5'-
168 GTGCAGTTTGTCTTTCCATCC-3'), 18S (sense: 5'-GTAACCCGTTGAACCCCATT-3'; antisense: 5'-
169 CCATCCAATCGGTAGTAGCG-3').
170
171 **Lentivirus production and transduction**
172 Lentiviral particles were produced by co-transfecting the envelope plasmid pCMV-VSV-G (Addgene),
173 packaging plasmid pCMV-dR8.2 dvpr (Addgene), and lentiCRISPRv2 (Addgene) or plentiCRISPRv2 with
174 UHRF gRNA (gRNA sequence: TCAATGAGTACGTCGATGCT; GenScript) into HEK293T cells using calcium
175 phosphate transfection method. Supernatants containing lentiviral particles were harvested at 24 hours
176 and 48 hours post-transfection. Cell debris were cleared by centrifugation at 1600 × g for 10 min at 4°C.
177 Supernatants were then filtered through 0.45 µm PES filter (25-223, Genesee Scientific), and
178 concentrated by ultracentrifugation at 23000 RPM for 2 hours at 4°C. Lentiviral particles were
179 resuspended in ice-cold PBS and stored at -80°C. Transduction of target cells were achieved by exposing

180 cells to viral particles in serum –free condition for 6 hours. Puromycin selection was carried out at a
181 concentration of 2 μg/ml.
182
183 **Clonogenic assay**
184 4% agarose stock was prepared by mixing agarose with water and kept warm in 55°C heat bath.
185 Appropriate cell culture medium was used for subsequent dilution of the agarose stock. 6-well plates
186 were coated with 1ml of 0.75% agarose prior to seeding. Single cell suspension was mixed with agarose
187 to achieve a final agarose concentration of 0.36%, the mixture was then layered on top of the 0.75%
188 agarose coating (Seeding density 200 cells/cm^2). Cells were incubated at 37°C with 5% CO_2 until cells in
189 control wells have formed sufficiently large colonies (>50 cells). Colonies were fixed with 10% methanol
190 for 15 min and stained with 5% Giemsa for 30 min for visualization.
191
192 **Immunocytochemistry**
193 Cell were seeded onto glass coverslips in a 24-well plate at a density of 25000 cells/well and allowed to
194 attach overnight. For EdU staining the Click-iT EdU cell proliferation kit (Thermo Fisher Scientific) was
195 used following manufacturer's instructions with 1 h pulse using a final 10 μM EdU solution in media. For
196 UHRF1 immunostaining, media was aspirated, and cells were fixed using 4% (w/v) paraformaldehyde
197 overnight at 4°C. Slides washed with PBS twice and then incubated with primary antibody overnight at
198 4°C. Mouse anti-UHRF1 antibody (PA5-29884, Thermo Fisher Scientific) was used at 1:500 dilution.
199 Slides washed 3 times in PBS then incubated with an anti-rabbit secondary antibody (BA-1000, Vector
200 Laboratories) in 1:500 dilution with corresponding blocking buffer for 30 minutes at room temperature
201 in the dark. Slides were washed 3 times with PBS and incubated in 300 μl of Vectastain ABC kit (Vector
202 Laboratories) for 30 minutes at room temperature. Slides were washed 3 times in PBS and incubated
203 with tyramide Cy3 1:150 in amplification buffer (Perkin Elmer) for 10 minutes. After washing with PBS

204 for 3 times, DAPI was added (1:1000 dilution in PBS) for 5 minutes to stain the nuclei. Slides were
205 washed twice with PBS and mounted using gelvatol containing DABCO. Imaging was completed using
206 Life Technologies EVOS microscope. Cell scoring was performed by a blinded investigator.
207
208 **Subcutaneous injection**
209 Human OS cell lines were dissociated in 0.25% trypsin-EDTA, washed with PBS prior to counting. $2 \cdot 10^6$
210 cells were resuspended in 100 µl of PBS and injected subcutaneously into the flank region of mice.
211 Tumors were collected 3 weeks post injection. For cells that require doxycycline induction for the
212 expression CRISPR/Cas9, 2 mg/ml doxycycline hyclate supplemented water was administered *ad libitum*.
213 10 mg/ml of sucrose was added to doxycycline supplemented water to increase consumption.
214
215 **RNA Sequencing**
216 Total RNA was isolated using the RNA Micro Kit (Qiagen). Subsequently, 500 ng of total RNA was used to
217 create the RNA-seq library following the manufacturer's protocol from purification, mRNA
218 fragmentation through the adenylation of end-repaired cDNA fragments and cleanup (TruSeq Stranded
219 mRNA, Illumina). The collected sample was cleaned with AMPure XP beads (Beckman Coulter) and
220 eluted in 20 µl of 10 mM Tris buffer, pH 8, 0.1% Tween 20. A paired-end 100-bp sequencing run was
221 performed on HiSeq 4000 yielding 348M PE reads with a final library concentration of 2 nM as
222 determined by qPCR (KAPA Biosystem).
223
224 Sequencing reads were aligned to the mouse or human reference genome (GRCm38 or GRCh38,
225 ENSEMBL v.92) using STAR (v2.5.2a) [24]. Each read pair was allowed a maximum number of
226 mismatches of 10. Each read was allowed a maximum number of multiple alignments of 3. Gene counts
227 for each sample were produced using HTSeq (v0.6.1p1) [25]. Read count normalization and differential

228 expression analysis were performed using DESeq2 (v1.22.2) in R (v3.5.2) [26]. Genes with low reads (sum
229 across samples < 10) were removed. Differentially expressed genes (DEG) were calculated by comparing
230 UHRF1 knockouts to matching controls, genes with base mean ≥ 10, Log2FoldChange ≥ 1 or ≤ -1, and
231 adjusted p value (Benjamini-Hockberg) ≤ 0.05 were called differentially expressed genes. 3D PCA plot
232 was generated using the R package plot3D (v1.1.1).
233
234 All sequencing data discussed in this publication have been deposited in NCBI's Gene Expression
235 Omnibus [27] and are accessible through GEO Series accession number GSE144418
236 (https://www.ncbi.nlm.nih.gov/geo/query/acc.cgi?acc=GSE144418).
237
238 **Scratch-wound assay**
239 Cells were seeded the day before the scratch at a density of $1.1\times10^5/cm^2$ and grown to 100% confluency
240 in 6-well cell culture plates. Two hours before the scratch, cells were treated with 5 µg/ml of mitomycin
241 C (S8146, Sigma). At time 0, a 1000 µl tip was used to create a wound across the cell monolayer. The
242 cells were then placed back to the incubator for 8 hours at 37°C with 5% CO_2. Images of the wound at
243 the exact same field were taken at 0 and 8 h and analyzed using the ZEISS ZEN microscope software. A
244 total of 10 measurements in pixels were made per image. The pixels migrated was calculated as the
245 difference between the average width of the scratches before and after the incubation period. p-values
246 were calculated using two-tailed t-test. Amiloride was used at 150 µM, BC 11 hydrobromide at 16.5 µM,
247 both were supplemented in growth medium and given to the cells at the 0 h time point.
248
249 **Transwell invasion assay**
250 PET track-etched membrane with 8µm pore (353097, Corning) were inserted into 24-well cell culture
251 plate. Membranes were coated with Matrigel at a density of 25 µg/insert. 2×10^4 cells were seeded onto

252 the membrane in 100 µl of appropriate cell culture medium and placed into the incubator for 2 hours at
253 37°C with 5% CO_2 to allow cell attachment. After the cells have attached to the membrane, 100 µl of
254 medium were added to the inner chamber, amiloride and BC11 hydrobromide were supplemented at
255 this time at 300 µM and 32.8 µM, respectively, to reach a final concentration of 150 µM and 16.4 µM. If
256 doxycycline is required, 2 µg/ml doxycycline was prepared in 100 µl medium in order to reach a final
257 concentration of 1 µg/ml. 600 µl of appropriate cell culture medium supplemented with 100 ng/ml
258 fibroblast growth factor (FGF) were pipetted into the outer chamber. Cells were then placed back into
259 the incubator for no more than 16 hours at 37°C with 5% CO_2. Cell culture medium was aspirated, and
260 cotton swabs were used to scrape off non-migratory cells on the top side of the insert. The remaining
261 cells at the bottom side of the insert were then fixed and stained with a solution consists of 6%
262 glutaraldehyde and 0.5% crystal violet for 2 hours. Stains were washed out with tap water and the
263 inserts left to dry at room temperature. Images of 5 different fields within each insert were taken for
264 analysis by cell count.
265
266 **Tail vein injection**
267 Human OS cells lines were dissociated in 0.25% trypsin-EDTA, washed with PBS prior to counting. For the
268 experimental metastasis model, 2×10^6 cells were resuspended in 200 µl of PBS and injected
269 intravenously through the tail vein. Mice lungs were collected 3 weeks after injection, fixed in 4%
270 formaldehyde for histological analysis.
271
272
273 **RESULTS**
274
275 **UHRF1 is overexpressed in mouse OS**

276 The developmental mouse model of OS using Osterix-driven Cre-recombinase (Osx-cre) to facilitate
277 preosteoblast-specific loss of *Tp53* results in tumor formation with complete penetrance and gene
278 expression profiles, histology, and metastatic potential comparable to that of human OS [28, 29]. Loss of
279 *Rb1* in addition to *Tp53* potentiates OS in these mice, strongly mimicking the behavior of the disease in
280 human. OS mice develop tumors with calcified interior and highly proliferative exterior, which can be
281 captured by microCT and FDG-PET scans, respectively (Figure 1A). Our previous work identified *UHRF1*
282 as a target that is overexpressed upon *RB1* inactivation and plays a significant role in the epigenetic
283 changes that drive tumor progression in retinoblastoma [17]. We found that UHRF1 is significantly
284 overexpressed in tumors arising from genetically engineered mouse models of OS. *In situ* hybridization
285 confirmed high levels of *UHRF1* mRNA in *Tp53* single conditional-knockout (cKO; *Osx-cre Tp53*$^{lox/lox}$) and
286 *Tp53*/*Rb1* double conditional-knockout (DKO; *Osx-cre Tp53*$^{lox/lox}$ *Rb1*$^{lox/lox}$) OS tumors (Figure 1B). These
287 high *UHRF1* transcript levels resulted in overexpressed protein levels in both *Tp53* cKO and *Tp53*/*Rb1*
288 DKO OS tumors compared to mouse mesenchymal stem cells (mMSC; Figure 1C).
289
290 **UHRF1 is a critical driver of the increased malignancy observed in *Rb1*-null OS**
291 In order to study the role of UHRF1 in OS development *in vivo*, we first assessed whether loss of *Uhrf1* in
292 osteogenic progenitors affected normal bone development. Since *Uhrf1* knockout mice result in mid-
293 gestational lethality [30], we generated mice with preosteoblast-specific knockout of *Uhrf1* (*Osx-cre*
294 *Uhrf1*$^{lox/lox}$). Bone density analyses of the femur, tibia, and humerus exhibited no difference in Hounsfield
295 units (n=4) upon preosteoblastic loss of *Uhrf1* (Figures 1D-E). Thus, *Uhrf1* loss does not appear to affect
296 normal bone development, independent of gender (Figure 1E).
297
298 We subsequently generated a series of genetically engineered mice to facilitate *Uhrf1* knockout in two
299 different strains of OS genetic background mice, *Tp53* cKO and *Tp53*/*Rb1* DKO, resulting in *Tp53*/*Uhrf1*

300 DKO (*Osx-cre Tp53*$^{lox/lox}$ *Uhrf1*$^{lox/lox}$) and *Tp53*/*Rb1*/*Uhrf1* triple knockout (TKO; *Osx-cre Tp53*$^{lox/lox}$ *Rb1*$^{lox/lox}$
301 *Uhrf1*$^{lox/lox}$). *Tp53*/*Uhrf1* DKO and *Tp53*/*Rb1*/Uhrf1 TKO mice were compared to their corresponding
302 littermate controls (*Tp53* cKO and *Tp53/Rb1* DKO, respectively) for the assessment of the role of UHRF1
303 in promoting OS development and metastasis. All genotypes analyzed led to the development of OS in
304 mice, but with distinct survival rates and disease presentation. *In situ* hybridization performed on the OS
305 mouse tumors confirmed a significant reduction of *Uhrf1* in *Tp53*/*Uhrf1* DKO and *Tp53*/*Rb1*/*Uhrf1* TKO
306 (Figure 1F). In line with previous reports, the loss of *Rb1* in *Tp53*/*Rb1* DKO mice resulted in a significantly
307 shorter median survival of 28.1 weeks (n=53) compared to 48.4 weeks in *Tp53* cKO mice (n=39,
308 p<0.0001; Figure 1G). Strikingly, genetic ablation of *Uhrf1* in *Tp53/Rb1/Uhrf1* TKO mice resulted in a
309 substantial increase in survival compared to *Tp53/Rb1* DKO mice, with a median survival of 46.9 weeks
310 (n=37; p<0.0001). The survival of *Tp53/Rb1/Uhrf1* TKO (46.9 weeks) at early time points was comparable
311 to that of *Tp53* cKO (48.4 weeks, p=0.0577, Gehan-Breslow-Wilcoxon test), suggesting that elevated
312 UHRF1 protein levels are critical for the poor prognosis associated with *Rb1* loss (Figure 1G). However, at
313 the late time points, the *Tp53/Rb1/Uhrf1* TKO and *Tp53* cKO survival curves become distinct from each
314 other (p=0.0126, Mantel-Cox test), suggesting that early UHRF1 overexpression is not the unique factor
315 contributing to *Rb1* loss-associated outcomes. Since three *Tp53/Rb1/Uhrf1* TKO mice had not acquired
316 tumors well beyond the average of the rest of their study group (> 69 weeks; Figure 1G), we performed
317 FDG-PET/microCT scans on them followed by autopsy. FDG-PET/microCT scans revealed no detectable
318 tumors (Supplemental Figure 1), which was further confirmed through autopsy. Most remarkable,
319 genetic ablation of *Uhrf1* also resulted in a significant reduction in pulmonary metastatic potential, with
320 only 10% occurrence rate of lung metastases in *Tp53/Rb1/Uhrf1* TKO compared to 40% observed in
321 *Tp53/Rb1* DKO mice. In addition to the reduced rate in metastatic incidence, a lighter burden of
322 metastatic nodules was also observed in *Tp53/Rb1/Uhrf1* TKO mice (data not shown).
323

324 Since increased *Uhrf1* mRNA and protein levels are also detected in *Tp53* cKO mouse tumors (Figures
325 1B-C), we also examined the effect of *Uhrf1* loss in the survival of *Tp53/Uhrf1* DKO compared to *Tp53*
326 cKO mice. We observed a significant increase in the median survival of *Tp53/Uhrf1* DKO mice (71.4
327 weeks; n=39), compared to *Tp53* cKO (n=39; p=0.0007, Gehan-Breslow-Wilcoxon test), but not in overall
328 survival (p=0.1189, Mantel-Cox test; Figure 1H). Interestingly, we found that all *Tp53* cKO mice analyzed
329 with earlier morbidity (< 60 weeks) presented tumors with increased *Uhrf1* mRNA levels, suggesting
330 spontaneous *RB1* inactivation, while only a third of tumors analyzed from mice that reached moribund
331 status later in life (>60 weeks) displayed *Uhrf1* overexpression (data not shown). Furthermore,
332 pathology analysis of histological sections for tumors from the four OS mouse models analyzed linked
333 *Uhrf1* loss with lower mitotic index and decreased anaplasia (Supplemental Figure 2 and Supplemental
334 Table 1).
335
336 Following the observation of the three *Tp53/Rb1/Uhrf1* TKO mice without detectable tumors, we sought
337 to determine if loss of *Uhrf1* contributed to delayed tumor promotion or decreased tumor progression.
338 To address this question, we performed periodic FDG-PET/microCT scans on *Tp53/Rb1* DKO and
339 *Tp53/Rb1/Uhrf1* TKO mice to determine the earliest age at which tumors could be detected (Figure 1I).
340 In *Tp53/Rb1* DKO mice, tumors were detected in average at 30.8 ± 2.9 weeks (n=4) while in
341 *Tp53/Rb1/Uhrf1* TKO mice, tumors were detected significantly later at 41.1 ± 6.6 weeks (n=4; p=0.0362;
342 Figure 1J). All test subjects reached humane end of study within 3 weeks of first tumor detection. These
343 data suggest that *Uhrf1* plays a pivotal role in OS tumor promotion following loss of *Rb1*.
344
345 **UHRF1 is overexpressed in human OS**
346 Following the observation of the critical role of UHRF1 overexpression contributing to the more
347 aggressive phenotype in OS mouse tumors, we next examined whether targeting UHRF1 would be

348 beneficial in human OS. Upon examination of The Cancer Genome Atlas (TCGA) database, we found that
349 *UHRF1* is significantly overexpressed in malignancies with frequently RB-pathway inactivation
350 presentation including sarcomas, breast invasive carcinomas, and lung adenocarcinomas; while tumors
351 where RB loss is infrequent in primary disease, such as prostate adenocarcinomas [31], show no
352 significant difference in *UHRF1* compared to control normal tissue (Figure 2A). *In situ* hybridization of a
353 human OS tissue array identified the presence of *UHRF1* mRNA in the 25 primary OS tumors examined
354 (Figure 2B). A larger proportion of samples expressing high *UHRF1* mRNA levels were classified as stage
355 II than stage I OS (Figure 2C), suggesting that UHRF1 expression increases in more aggressive tumors.
356 However, the limited number of stage III and stage IV samples available restricted our analysis of
357 metastatic cases. Given the interesting possibility of a role of UHRF1 in OS metastasis shown by our
358 mouse models, we analyzed *UHRF1* expression using a published RNA-Seq dataset of pretreatment
359 biopsies from 53 high-grade OS patients who did or did not develop metastasis within 5 years, compared
360 to normal mesenchymal stem cells (MSC), and osteoblasts [32]. The *UHRF1*expression levels found in
361 MSCs (log2 median = 9.055) were not significantly different than osteoblasts (log2 median = 8.510;
362 p=0.1495) nor tumors from patients that did not develop metastasis within 5 years from the time of
363 biopsy (log 2 median = 9.055; p=0.1123). However, tumors from patients who developed metastasis
364 within 5 years from the time of biopsy expressed significantly higher levels of *UHRF1* (log2 mean = 9.880;
365 p = 0.0015; Figure 2D).
366
367 The clinical data led us to examine UHRF1 mRNA and protein levels in 4 different human OS cell lines:
368 143B, SJSA-1, SaOS-2 (RB-null cell line), and U-2 OS, along with 5 patient-derived orthotopic xenografts
369 (PDX1-5). qPCR analysis of human OS cell lines and PDX showed a significant upregulation of *UHRF1*
370 mRNA levels in all samples except PDX2 when compared to human mesenchymal stem cells (MSC),
371 independent of whether they express RB protein or not (Figure 2E-F and Supplemental Figure 3A). At the

372 protein level, UHRF1 was highly overexpressed across all analyzed OS subjects compared to MSC
373 controls (Figure 2G-H).
374
375 ***UHRF1* is a direct target of the RB/E2F signaling pathway in the osteogenic lineage**
376 A few studies have reported UHRF1 as a direct E2F1 transcriptional target [33, 34]. Following our
377 observations that UHRF1 is overexpressed in all OS samples analyzed, we aimed to confirm whether
378 UHRF1 is a direct E2F1 target in the osteogenic lineage. We performed chromatin immunoprecipitation
379 (ChIP) analysis in MSC and found E2F1 enrichment at E2F1 consensus binding motifs located within the
380 UHRF1 promoter (Supplemental Figure 3B). To confirm E2F1 drives *UHRF1* transcription in OS cells, we
381 knockdown of E2F1 using shRNA, which resulted in a modest decrease in UHRF1 protein levels in OS cell
382 lines (data not shown). Knockdown of E2F1 in combination with E2F3, but not in combination with E2F2,
383 significantly decreased UHRF1 protein levels (Supplemental Figure 3C and data not shown). We verified
384 that UHRF1 expression is transcriptionally regulated by the canonical RB/E2F pathway, by treating
385 human OS cell lines with the CDK4/6 inhibitor, palbociclib, to inhibit RB hyperphosphorylation and
386 thereby, limiting active E2F. qPCR analysis revealed significant decreases in *UHRF1* mRNA levels upon
387 palbociclib treatment, with the exception of the RB-null cell line, SaOS-2, which served as a negative
388 control (Supplemental Figure 3D). Palbociclib treatment also decreased UHRF1 protein levels in a dose-
389 dependent manner in RB-positive OS cells, as revealed by Western Blot analysis (Supplemental Figure
390 3E). In line with these results, we also observed an upregulation of *CDK4* and/or *CDK6* transcripts in RB-
391 wildtype OS cell lines and/or *INK4A* downregulation (Supplemental Figure 3H-I). Indeed, SJSA-1 is known
392 to have *CDK4* amplification and U2-OS to have *INK4A* deletion. Together, these data confirmed
393 transcriptional regulation of *UHRF1* by the RB/E2F pathway through direct transcriptional activation by
394 activator E2Fs, E2F1 and E2F3.
395

396 **UHRF1 promotes human OS cell proliferation *in vitro* and *in vivo***

397 Emerging reports have linked UHRF1 overexpression in cancer with its ability to promote proliferation,
398 migration/invasion, or both [17, 35-40]. To study the role of UHRF1 overexpression in OS, we first
399 generated UHRF1-knockdown OS cell lines using shRNA; however, we discovered that UHRF1
400 knockdown cannot be sustained for more than two weeks, challenging the reproducibility of our results
401 over time (data not shown). To overcome this challenge, we generated lentiviral CRISPR vectors
402 encoding gRNA sequence complimentary to UHRF1 to facilitate UHRF1 gene knockout (KO) in OS cell
403 lines, as well as non-targeting vector control (VC). Single clones (n=3) were selected for SJSA-1 and 143B,
404 while the other cell lines remained as pools and were analyzed within 2-3 weeks after being generated.
405 Western blot analysis revealed successful UHRF1 KO in all four OS cell lines tested (Figure 3A). To assess
406 whether UHRF1 is required for OS cell proliferation, we first performed growth curve analysis, and found
407 that UHRF1 KO cells displayed longer doubling times compared to VC OS cells (Figure 3B). The decrease
408 in proliferation potential was further evidenced through clonogenic assays (Figure 3C). UHRF1 loss
409 decreased the OS cells' ability to give rise to colonies at a single cell level, as seen by a significant
410 reduction in both the number and the size of colonies in UHRF1 KO compared to VC cells; except for
411 SaOS-2, where we observed a decrease in number and size but the magnitude of the change did not
412 reach statistical significance (Figure 3D). To directly assess cell proliferation, we pulsed UHRF1 KO and
413 VC cells with EdU, a thymidine nucleoside analog, for 1 h, to label actively proliferating cells (Figure 3E).
414 We found that UHRF1 KO cells had reduced EdU incorporation, as seen by the significantly lower
415 percentage of EdU-positive cells when compared to VC, suggesting a slower rate of active DNA synthesis;
416 with the exception of U-2 OS, albeit a trend of decreased incorporation was still observed (Figure 3F).

417

418 UHRF1 depletion also has been reported to sensitize cancer cells to chemotherapeutic drugs [41, 42].
419 We evaluated whether UHRF1 loss in OS cells would alter their sensitivity to standard-of-care drugs,

420 doxorubicin, cisplatin and methotrexate. As observed from the dose-response curves generated using
421 the Cell TiterGlo viability assay, we found moderate reduction in drug sensitivity in UHRF1 KO cells in
422 comparison to VC, evidenced by mild increases in EC50. This holds true for both single agent treatment
423 and combination treatment (Supplemental Figure 4). Although diverging from previous reports, these
424 observations are consistent with the decreased proliferation rate seen in KO cells and the mechanism of
425 action of these drugs, which are more efficacious in reducing viability of cells with higher proliferation
426 rates.
427
428 To assess proliferative capacity *in vivo*, UHRF1 KO and VC OS cells were injected subcutaneously into
429 immune-deficient mice at either flank regions. UHRF1 KO cells gave rise to tumors with significantly
430 lighter burden when compared to VC. Tumors formed from UHRF1 KO cells reached an average size of
431 0.49 ± 0.37 cm^3 and an average weight of 0.70 ± 0.69 g compared to an average volume of 1.233 ± 0.75
432 cm^3 (p=0.02, n=10) and average weight of 1.62 ± 1.09 g (p=0.01, n=10) from tumors formed by VC cells.
433 To test the therapeutic potential of targeting UHRF1 in established tumors, we utilized a doxycycline-
434 inducible system to drive the expression of CRISPR gRNA against UHRF1. Inducible UHRF1 KO and VC OS
435 cells were subcutaneously injected and tumors were allowed to establish for one week, followed by the
436 induction of CRISPR/Cas-9 gRNAs using orally delivered doxycycline (Figure 3G). Tumor growth was
437 significantly reduced in UHRF1 KO tumors, with an average tumor volume of 0.356 ± 0.201 cm^3
438 compared to 1.455 ± 0.865 cm^3 in VC tumors (p=0.02; n=5; Figure 3H-I). The average tumor weight was
439 also reduced, with UHRF1 KO tumors averaging 0.46 ± 0.45 g compared to 1.80 ± 1.11 g in VC tumors
440 (p=0.01, n=5; Figure 3I). Western blot was performed to confirm the decrease in UHRF1 in UHRF1 KO
441 tumors (Figure 3K). UHRF1 KO tumors also presented phenotypic features of less aggressive tumors, as
442 seen by lessened vasculature and ulceration compared to tumors formed from VC cells (Figure 3J).
443 Taken together, both *in vitro* and *in vivo* data suggest that UHRF1 is critical for OS cell proliferation.

444

445 **UHRF1 promotes human OS cell migration and invasion *in vitro* and *in vivo***

446 The high metastatic potential of OS is the main cause of mortality in patients. Given that our mouse
447 models indicated a possible involvement of UHRF1 in OS metastasis, we sought to evaluate the role of
448 UHRF1 in promoting cell migration, invasion, and metastasis. Scratch-wound assay was carried out to
449 assess the migratory potential of UHRF1 KO OS cell lines (Figure 4A). We observed a significant decrease
450 in the distance migrated in UHRF1 KO compared to VC OS cells for all cell lines studied, with an average
451 of 56.8 ± 2.3% reduction in migration across the three cell lines (Figure 4B). In addition to the decrease
452 in migratory potential, Transwell invasion assays revealed a significant reduction in the number of
453 UHRF1 KO OS cells capable of mobilizing across Matrigel-coated inserts in all OS cell lines (Figures 4C-D).

454

455 Finally, to test whether the reduced migratory and invasive capacities *in vitro* translate into less
456 metastatic potential *in vivo*, we injected SJSA-1 UHRF1 KO and VC cells into the tail vein of immune-
457 deficient mice and assessed the rate of lung colonization 3-weeks post injection. We found that the
458 lungs of mice injected with UHRF1 KO cells had a reduced number of metastatic nodules and a
459 significantly reduced tumor nodule size when compared to the lungs of mice injected with VC cells
460 (Figures 4E-G). We also observed a significant decrease in the burden of lung metastases when we
461 injected inducible SJSA-1 UHRF1 KO into the tail-vein of mice fed with doxycycline, compared to VC cells
462 (Figures 4H-J), as reflected by significant decrease of total lung weight (data not shown) and reduced
463 number (I) and size (J) of metastatic nodules. This suggests that targeting UHRF1 would be an effective
464 strategy to reduce metastases even when tumor cells have already undergone intravasation.

465

466 **UHRF1 overexpression promotes human MSC cell migration and invasion**

467 In order to conclusively associate UHRF1 overexpression with cell migration, we performed gain-of-
468 function studies using MSCs, the normal progenitor of the osteogenic tissue. For this, we generated a
469 doxycycline-inducible lentiviral vector system to drive UHRF1 overexpression (pCW57-UHRF1; Figure 5A)
470 and used the empty backbone vector as control (pCW57-VC). Western blot analysis was performed to
471 validate successful induction of UHRF1 overexpression upon doxycycline treatment in transduced MSCs
472 (Figure 5B). We observed that the rate of cell proliferation upon induction of UHRF1 overexpression in
473 MSCs was indistinguishable from doxycycline-induced VC (data not shown). Nonetheless, we found that
474 UHRF1 overexpression in MSCs significantly increased migratory potential as evidenced by the
475 significant increase in the distance migrated upon doxycycline induction in pCW57-UHRF1 cells
476 compared to pCW57-VC using scratch-wound assay (Figures 5C-D). Furthermore, induction of UHRF1
477 overexpression also led to a significant increase in the number of cells invaded across Matrigel-coated
478 Transwell membranes (Figures 5E-F).
479
480 **UHRF1 affects the expression of genes involved in cell migration and invasion**
481 UHRF1 is required for maintenance of DNA methylation during DNA replication through the recruitment
482 of DNMT1 [43]. However, UHRF1 ubiquitin ligase activity also targets DNMT1 for degradation, with some
483 studies reporting that UHRF1 overexpression results in decreased DNA methylation [44, 45]. To
484 determine the effects of UHRF1 loss on DNA methylation, chromatin structure, and transcription, we
485 analyzed global DNA methylation, chromatin accessibility, and transcriptome. We probed genomic DNA
486 isolated from UHRF1 KO and VC cell lines with an antibody against 5-methyl cytosine (5meC) to assess
487 global DNA methylation. We found genomic 5meC levels were decreased in UHRF1 KO compared to VC
488 across all but one OS cell lines examined (Supplemental Figure 5A).
489

490 We also analyzed changes in the chromatin landscape upon loss of UHRF1 by performing ATAC-seq in
491 143B, SJSA-1, and SaOS-2 UHRF1 KO compared to VC (Supplemental Figure 5B). Despite the role of
492 UHRF1 in heterochromatin maintenance and the decreased genomic levels in DNA methylation, we
493 identified only 16 chromatin regions with significant changes in chromatin accessibility across these 3
494 biological replicates (Supplemental Table 2). Within these changes, the majority were consistent with
495 the role of UHRF1 chromatin repression, with approximately 69% (11/16) resulting in opening of
496 chromatin upon UHRF1 loss.
497
498 In line with modest changes in chromatin accessibility, gene expression analysis using RNA-seq revealed
499 that the gene expression profile from UHRF1 KO cell lines present minor variability from VC cells, as
500 portrayed by the principal component analysis (PCA) plot (Figure 6A). We identified only a total of 272
501 differentially expressed genes (DEGs), with 191 upregulated genes and 81 downregulated genes in
502 UHRF1 KO compared to VC cells. The predominance of gene upregulation upon *UHRF1* loss is consistent
503 with the reduction in DNA methylation levels. Given the lack of chromatin accessibility changes
504 observed in ATAC-seq, changes in DNA methylation that may affect gene expression are likely affecting
505 transcription factor binding rather than chromatin relaxation at these promoter. Of particular interest,
506 gene ontology (GO) analysis for biological processes of these 272 DEGs showed an enrichment of genes
507 involved in regulation of cell migration and cellular adherence, as seen by the classification of the top 10
508 most significant GO terms (Figure 6B). We confirmed the changes in gene expression observed among
509 top 13 genes involved in regulation of cell migration (Figure 6C) through qPCR (Figure 6D and data not
510 shown).
511
512 **Urokinase plasminogen activator contributes to OS migration downstream of UHRF1**

513 Plasminogen activator, Urokinase (*PLAU*) was one of the genes identified through the transcriptome
514 analysis to be potentially involved in UHRF1-mediated cell migration. Significant decrease in the levels of
515 the *PLAU* transcript were observed in UHRF1 KO OS cells (Figure 6D), as well as the tumors they form
516 subcutaneously in immune-deficient mice, with an average 2.2-fold decrease when compared to tumors
517 formed from VC cells (p=0.038, Figure 6E). Thus, we tested whether treatment with amiloride, an
518 inhibitor for the urokinase-type plasminogen activator (uPA) protein encoded by *PLAU*, could decrease
519 migratory potential and invasiveness of OS cells. Scratch-wound assays of amiloride treated OS cell lines
520 showed a significant decrease in migratory potential, with an average of 40.3 ± 11.9% decrease across all
521 OS cell lines examined (Figure 7A). Significant decrease of invasiveness, as determined by Transwell
522 invasion assay, is also observed upon amiloride treatment (Figure 7B-C), confirming uPA as an important
523 contributor of OS migratory potential. In line with our observations associating UHRF1 with uPA levels,
524 amiloride treatment was able to inhibit UHRF1-induced cell migration in MSCs (Figure 7D-E). BC 11
525 hydrobromide, a selective uPA inhibitor, was used to further verify the role of uPA in OS cell migration. A
526 23.2 ± 10.2% decrease in migration is seen across OS cell lines upon treatment (Figure 7F). Taken
527 together, we established a positive correlation between UHRF1 expression levels and migration/invasion
528 potential in the osteogenic lineage, with uPA as the potential conduit between the two.
529
530
531 **DISCUSSION**
532 Metastasis remains the most frequent fatal complication of OS. The lack of significant breakthroughs
533 beyond the scope of standard chemotherapeutics targeting highly proliferative underscores a pressing
534 clinical need for new therapeutic strategies for OS. For decades, genetic alterations at the *RB1* gene
535 have been associated with increased mortality, metastasis and poor response to chemotherapy in
536 osteosarcoma [7-11, 46, 47]. However, the precise mechanism through which this occurs remains to be

537 elucidated in order to develop better therapeutic strategies. In this study, we identified *UHRF1* as a
538 direct target of RB/E2F pathway. UHRF1 overexpression is directly correlated with increased OS
539 malignancy and metastatic disease in humans. Specifically, UHRF1 facilitates OS cell proliferative,
540 invasive, and metastatic capacity. Most importantly, we found that the decrease in survival associated
541 with loss-of-function mutations at the *Rb1* gene is critically mediated through the overexpression of
542 UHRF1.
543
544 Studies from retinoblastoma, a cancer initiated by biallelic inactivation of the *RB1* gene, defined a
545 central role of RB in epigenetic control and a key role of RB/E2F-regulated chromatin remodelers in
546 tumorigenesis [16, 17, 48]. Among these chromatin remodelers, UHRF1 was identified as a potential
547 critical regulator of tumor initiation and progression following RB-pathway deregulation that is
548 overexpressed in several cancers [17-21]. We confirmed *UHRF1* upregulation in human OS cell lines,
549 PDXs, and primary OS tissue. Further, UHRF1 protein overexpression is recapitulated in both *p53* cKO
550 and *Tp53*/*Rb1* DKO OS mouse model, validating the suitability of this mouse model for the study of OS.
551 Direct regulation of UHRF1 by the RB/E2F signaling pathway was described previously, though in limited
552 context [33, 34]. We established that *UHRF1* expression is transcriptionally regulated by the RB/E2F
553 signaling pathway in the osteogenic lineage. ChIP analysis revealed enrichment of E2F1 at putative
554 binding motifs within the promoter region of *UHRF1*. However, E2F1 knockdown was insufficient in
555 reducing UHRF1 expression. Rather, significant reduction of UHRF1 level was achieved only through
556 combined knockdown of E2F1 and E2F3, suggesting compensatory mechanisms between activator E2Fs
557 in regulating the transcription of downstream targets. As the RB/E2F signaling pathway is often
558 inactivated in cancer through mechanisms other than *RB1* loss-of-function mutations, the most common
559 being RB hyperphosphorylation through CDK4/6 activation or p16 inactivation [49-51], it is not
560 surprising that UHRF1 upregulation and overexpression in OS is not restricted to *RB1*-null cases. UHRF1

561 overexpression in *RB1*-wildtype OS cell lines can be explained by upregulation of *CDK4* and/or *CDK6*,
562 which leads to RB hyperphosphorylation, preventing the repression of E2F binding activities. Increased
563 CDK4/6 activity being the predominant mechanism of pathway inactivation in OS is further confirmed by
564 the down-regulation of *UHRF1* and dose-dependent decrease of UHRF1 upon treatment with palbociclib,
565 a known CDK4/6 inhibitor [52].
566
567 UHRF1 expression is positively correlated with cell proliferation and cell mobility in both normal and
568 malignant cells *in vitro* [17, 37-40]. Although it is clear that UHRF1 expression is linked to cellular
569 phenotypes that strongly associate with tumor malignancy, the link between UHRF1, OS tumor
570 progression, and its role in the poor prognosis associated with *RB1* loss has not been established. Our
571 results showed that UHRF1 KO decreases clonogenicity and tumor growth both *in vitro* and *in vivo*.
572 Independent from its role on proliferation, UHRF1 has a clear effect on the migratory potential of the
573 osteoblastic lineage as UHRF1 overexpression was sufficient to increase migration and invasion of
574 normal MSCs and targeting UHRF1 drastically reduced migration, invasion and metastatic capacity of OS
575 cell lines. It is important to note that although RB-null status has been clinically associated with poor
576 disease outlook, the RB-null cell line, SaOS-2, does not exhibit higher aggressiveness in comparison to
577 other cell lines. This could be explained by the limitation of utilizing cell lines, in which loss of clinical
578 representation is commonly seen. Our results also suggest that uPA is critical for this UHRF1-mediated
579 migration. uPA is a serine protease that has long been associated with tumor malignancy. Upon
580 conversion of plasminogen into plasmin, uPA triggers a proteolytic cascade that leads to the degradation
581 of extracellular matrix, an event necessary for angiogenesis and metastasis. Our findings are in line with
582 a previous study describing the uPA/uPAR axis as a metastatic driver in OS [53]. While our results
583 suggest that targeting UHRF1 might result in a more robust therapeutic outcome, the observation that

584 the UHRF1 induced cell migration can be reversed by treatment with uPA inhibitors like amiloride [54]
585 and BC11 hydrobromide, provides a therapeutic alternative that can be further explored immediately.
586
587 Our group is the first to model the critical role of UHRF1 in osteosarcomagenesis, with *Uhrf1* KO
588 resulting in a dramatic increase in overall survival and decrease in metastases, particularly in *Rb1*-null OS.
589 Indeed, median survival and rate of metastasis of *Tp53*/*Rb1*/*Uhrf1* TKO closely resembled that of *Tp53*
590 cKO mice, indicating that UHRF1 is a major driver of *Rb1* loss-associated malignancy. Interestingly, our
591 results also indicate that the increased survival in *Tp53*/*Rb1*/*Uhrf1* TKO mice is largely a result of delayed
592 tumor promotion, with negligible differences in tumor growth rates once the tumors have been
593 detected. This is quite distinct from our observations targeting UHRF1 in established tumor cells,
594 suggesting there might be compensatory pathways arising in the developmental tumor models. Further
595 studies on tumors arising from these developmental OS models might provide insight on potential
596 compensatory mechanisms of *Uhrf1* loss which may be relevant for predicting mechanisms of resistance
597 for future UHRF1-targeted therapeutics.
598
599 While targeting *Uhrf1* in developmental mouse models showed a distinct improvement in survival in
600 *Rb1*-null tumors over *Rb1*-wildtype, such distinctions were not observed in UHRF1 overexpressing
601 human OS cell lines. Both *RB1*-null and *RB1*-wildtype OS cell lines appear to equally benefit from
602 targeting UHRF1. It is possible that the timing of UHRF1 overexpression is crucial for the resulting poor
603 prognosis. Early *Rb1* loss would result in immediate UHRF1 overexpression which quickly promotes
604 tumorigenesis compared to tumors that eventually inactivate the RB/E2F pathway through alternative
605 mechanisms. Supporting this theory, *Tp53/Uhrf1* DKO mice showed some improvement in survival
606 compared to the more aggressive *Tp53* cKO mice that showed RB/E2F pathway inactivation.
607 Alternatively, the RB/E2F complex is known not only for its role in direct transcriptional repression, but

608 also as epigenetic modifiers through the recruitment of chromatin remodelers [12-16]. Two UHRF1
609 domains, PHD and RING, contain LXCXE RB-binding motifs [55]. Our unpublished data shows UHRF1
610 preferentially binds to hyperphosphorylated RB. Thus, *RB1*-wildtype OS cells may preserve protein-
611 protein interactions and RB regulation on UHRF1. The possible loss of this layer of regulation in *RB1*-null
612 tumors could account for the drastic difference in clinical prognosis, supporting the view that the
613 inactivation of RB by phosphorylation is not functionally equivalent to the mutation of the *RB1* gene [56].
614 Unpublished data from our group strongly supports a critical role of UHRF1 in aiding RB-mediated
615 tumorigenesis, with loss of *Uhrf1* completely abrogating tumor formation in an *Rb1/p107* knockout
616 model of retinoblastoma and significantly increasing survival of a *Tp53/Rb1* model of small cell lung
617 cancer, similar to the observations presented for osteosarcoma in this study.
618
619 To summarize, our study provided multifaceted evidences both *in vitro* and *in vivo* supporting UHRF1
620 targeting as a novel therapeutic strategy in treating OS. The involvement of UHRF1 in OS cell
621 proliferation and its critical role in tumor promotion strongly outweighs the mild desensitization of OS to
622 standard care therapeutics. We showed that UHRF1 targeting holds great potential in overcoming the
623 highly metastatic characteristic of OS, the main reason why survival rate has remained stagnant in past
624 decades. We stand to be the first to model the effect of UHRF1 throughout development and showed
625 minimal on-target toxicity, as opposed to various chemotherapeutic agents known to affect bone
626 homeostasis [57]. Moreover, the degree to which UHRF1 loss reverted the increased malignancy upon
627 *Rb1* loss suggests that the benefit of UHRF1 targeting could go beyond the scope of OS by improving
628 current treatment paradigms of other cancers harboring RB/E2F pathway inactivation.
629
630
631 **ACKNOWLEDGEMENTS**

632 We thank Erin Yamanaka, Josselyn Peña, Sara Akhlaghi, and Annie Jeon for help with mouse genotyping
633 and cell culture; Makena Ewald for chemotherapeutic dose-response curves; Christopher Liang for help
634 with FDG-PET/microCT scans; Dr. Ali Nael, Dr. Robert Edwards and Dr. Aaron Sassoon for assistance with
635 pathology analysis. This work was supported in part by grants to C.A.B. from the NIH (CA178207 and
636 CA229696), the American Cancer Society (129801-IRG-16-187-13 and 133403-RSG-19-031-01-DMC) and
637 the 2018 AACR-Aflac, Inc. Career Development Award for Pediatric Cancer Research (18-20-10-BENA).
638 This work was also made possible, in part, through access to the Genomics High Throughput Facility
639 Shared Resource of the Cancer Center Support Grant (P30CA-062203) at the University of California,
640 Irvine and NIH shared instrumentation grants 1S10RR025496-01, 1S10OD010794-01, and
641 1S10OD021718-01.

642

643 *Authors contributions:* C.A.B. conceived the project. S.C.W., J.L., K.S., L.Z., and C.A.B. performed the
644 experiments. J.W. performed the sequencing data analysis. A.N. performed the pathology analysis. S.W.
645 and C.A.B. wrote the manuscript.

646

647 **References**

648 1. Cormier, J.N. and R.E. Pollock, *Soft tissue sarcomas.* CA Cancer J Clin, 2004. **54**(2): p. 94-109.
649 2. Ottaviani, G. and N. Jaffe, *The epidemiology of osteosarcoma.* Cancer treatment and research,
650 2009. **152**: p. 3-13.
651 3. Huang, Y.M., et al., *The metastasectomy and timing of pulmonary metastases on the outcome of*
652 *osteosarcoma patients.* Clin Med Oncol, 2009. **3**: p. 99-105.
653 4. Mirabello, L., R.J. Troisi, and S.A. Savage, *Osteosarcoma Incidence and Survival Rates From 1973*
654 *to 2004 Data From the Surveillance, Epidemiology, and End Results Program.* Cancer, 2009.
655 **115**(7): p. 1531-1543.
656 5. Martin, J.W., J.A. Squire, and M. Zielenska, *The genetics of osteosarcoma.* Sarcoma, 2012. **2012**:
657 p. 627254.
658 6. Chen, X., et al., *Recurrent somatic structural variations contribute to tumorigenesis in pediatric*
659 *osteosarcoma.* Cell Rep, 2014. **7**(1): p. 104-12.
660 7. Feugeas, O., et al., *Loss of heterozygosity of the RB gene is a poor prognostic factor in patients*
661 *with osteosarcoma.* J Clin Oncol, 1996. **14**(2): p. 467-72.
662 8. Benassi, M.S., et al., *Altered G1 phase regulation in osteosarcoma.* Int J Cancer, 1997. **74**(5): p.
663 518-22.
664 9. Goto, A., et al., *Association of loss of heterozygosity at the p53 locus with chemoresistance in*
665 *osteosarcomas.* Jpn J Cancer Res, 1998. **89**(5): p. 539-47.
666 10. Wadayama, B., et al., *Mutation spectrum of the retinoblastoma gene in osteosarcomas.* Cancer
667 Res, 1994. **54**(11): p. 3042-8.
668 11. Ren, W. and G. Gu, *Prognostic implications of RB1 tumour suppressor gene alterations in the*
669 *clinical outcome of human osteosarcoma: a meta-analysis.* Eur J Cancer Care (Engl), 2017. **26**(1).
670 12. Chi, P., C.D. Allis, and G.G. Wang, *Covalent histone modifications--miswritten, misinterpreted and*
671 *mis-erased in human cancers.* Nat Rev Cancer. **10**(7): p. 457-69.
672 13. Lu, J., et al., *A genome-wide RNA interference screen identifies putative chromatin regulators*
673 *essential for E2F repression.* Proc Natl Acad Sci U S A, 2007. **104**(22): p. 9381-6.
674 14. Benetti, R., et al., *A mammalian microRNA cluster controls DNA methylation and telomere*
675 *recombination via Rbl2-dependent regulation of DNA methyltransferases.* Nat Struct Mol Biol,
676 2008. **15**(9): p. 998.
677 15. Wen, H., et al., *Epigenetic regulation of gene expression by Drosophila Myb and E2F2-RBF via the*
678 *Myb-MuvB/dREAM complex.* Genes Dev, 2008. **22**(5): p. 601-14.
679 16. Zhang, J., et al., *A novel retinoblastoma therapy from genomic and epigenetic analyses.* Nature,
680 2012. **481**(7381): p. 329-34.
681 17. Benavente, C.A., et al., *Chromatin remodelers HELLS and UHRF1 mediate the epigenetic*
682 *deregulation of genes that drive retinoblastoma tumor progression.* Oncotarget, 2014. **5**(20): p.
683 9594-9608.
684 18. Mousli, M., et al., *ICBP90 belongs to a new family of proteins with an expression that is*
685 *deregulated in cancer cells.* British journal of cancer, 2003. **89**(1): p. 120-7.
686 19. Unoki, M., et al., *UHRF1 is a novel molecular marker for diagnosis and the prognosis of bladder*
687 *cancer.* Br J Cancer, 2009. **101**(1): p. 98-105.
688 20. Daskalos, A., et al., *UHRF1-mediated tumor suppressor gene inactivation in nonsmall cell lung*
689 *cancer.* Cancer, 2011. **117**(5): p. 1027-37.
690 21. Kofunato, Y., et al., *UHRF1 expression is upregulated and associated with cellular proliferation in*
691 *colorectal cancer.* Oncol Rep, 2012. **28**(6): p. 1997-2002.
692 22. Stewart, E., et al., *The Childhood Solid Tumor Network: A new resource for the developmental*
693 *biology and oncology research communities.* Dev Biol, 2016. **411**(2): p. 287-293.

694 23. Benavente, C.A., et al., *Cross-species genomic and epigenomic landscape of retinoblastoma.*
695 Oncotarget, 2013. **4**(6): p. 844-59.
696 24. Dobin, A., et al., *STAR: ultrafast universal RNA-seq aligner.* Bioinformatics, 2013. **29**(1): p. 15-21.
697 25. Anders, S., P.T. Pyl, and W. Huber, *HTSeq--a Python framework to work with high-throughput*
698 *sequencing data.* Bioinformatics, 2015. **31**(2): p. 166-9.
699 26. Love, M.I., W. Huber, and S. Anders, *Moderated estimation of fold change and dispersion for*
700 *RNA-seq data with DESeq2.* Genome Biol, 2014. **15**(12): p. 550.
701 27. Edgar, R., M. Domrachev, and A.E. Lash, *Gene Expression Omnibus: NCBI gene expression and*
702 *hybridization array data repository.* Nucleic Acids Res, 2002. **30**(1): p. 207-10.
703 28. Walkley, C.R., et al., *Conditional mouse osteosarcoma, dependent on p53 loss and potentiated by*
704 *loss of Rb, mimics the human disease.* Genes Dev, 2008. **22**(12): p. 1662-76.
705 29. Berman, S.D., et al., *Metastatic osteosarcoma induced by inactivation of Rb and p53 in the*
706 *osteoblast lineage.* Proceedings of the National Academy of Sciences of the United States of
707 America, 2008. **105**(33): p. 11851-6.
708 30. Muto, M., et al., *Targeted disruption of Np95 gene renders murine embryonic stem cells*
709 *hypersensitive to DNA damaging agents and DNA replication blocks.* J Biol Chem, 2002. **277**(37):
710 p. 34549-55.
711 31. Aparicio, A., R.B. Den, and K.E. Knudsen, *Time to stratify? The retinoblastoma protein in*
712 *castrate-resistant prostate cancer.* Nat Rev Urol, 2011. **8**(10): p. 562-8.
713 32. Kuijjer, M.L., et al., *Identification of osteosarcoma driver genes by integrative analysis of copy*
714 *number and gene expression data.* Genes Chromosomes Cancer, 2012. **51**(7): p. 696-706.
715 33. Magri, L., et al., *E2F1 coregulates cell cycle genes and chromatin components during the*
716 *transition of oligodendrocyte progenitors from proliferation to differentiation.* The Journal of
717 neuroscience : the official journal of the Society for Neuroscience, 2014. **34**(4): p. 1481-93.
718 34. Unoki, M., T. Nishidate, and Y. Nakamura, *ICBP90, an E2F-1 target, recruits HDAC1 and binds to*
719 *methyl-CpG through its SRA domain.* Oncogene, 2004. **23**(46): p. 7601-10.
720 35. Guan, D., et al., *The epigenetic regulator UHRF1 promotes ubiquitination-mediated degradation*
721 *of the tumor-suppressor protein promyelocytic leukemia protein.* Oncogene, 2013. **32**(33): p.
722 3819-3828.
723 36. Zhang, Y., et al., *Upregulated UHRF1 Promotes Bladder Cancer Cell Invasion by Epigenetic*
724 *Silencing of KiSS1.* PLoS One, 2014. **9**(10): p. Article No.: e104252.
725 37. Zhang, Z.-Y., et al., *Clinicopathological analysis of UHRF1 expression in medulloblastoma tissues*
726 *and its regulation on tumor cell proliferation.* Medical Oncology (Totowa), 2016. **33**(9): p. Article
727 No.: 99.
728 38. Zhu, M., et al., *Regulation of UHRF1 by microRNA-9 modulates colorectal cancer cell*
729 *proliferation and apoptosis.* Cancer Science, 2015. **106**(7): p. 833-839.
730 39. Cui, L., et al., *Up-regulation of UHRF1 by oncogenic Ras promoted the growth, migration, and*
731 *metastasis of pancreatic cancer cells.* Molecular and Cellular Biochemistry, 2015. **400**(1-2): p.
732 223-232.
733 40. Li, X.-L., et al., *Exogenous expression of UHRF1 promotes proliferation and metastasis of breast*
734 *cancer cells.* Oncology Reports, 2012. **28**(1): p. 375-383.
735 41. He, H., C. Lee, and J.K. Kim, *UHRF1 depletion sensitizes retinoblastoma cells to chemotherapeutic*
736 *drugs via downregulation of XRCC4.* Cell Death Dis, 2018. **9**(2): p. 164.
737 42. Fang, L., et al., *Gene therapy with RNAi targeting UHRF1 driven by tumor-specific promoter*
738 *inhibits tumor growth and enhances the sensitivity of chemotherapeutic drug in breast cancer in*
739 *vitro and in vivo.* Cancer Chemother Pharmacol, 2012. **69**(4): p. 1079-87.
740 43. Bostick, M., et al., *UHRF1 plays a role in maintaining DNA methylation in mammalian cells.*
741 Science, 2007. **317**(5845): p. 1760-4.

742 44. Du, Z., et al., *DNMT1 stability is regulated by proteins coordinating deubiquitination and*
743 *acetylation-driven ubiquitination.* Sci Signal, 2010. **3**(146): p. ra80.
744 45. Mudbhary, R., et al., *UHRF1 overexpression drives DNA hypomethylation and hepatocellular*
745 *carcinoma.* Cancer Cell, 2014. **25**(2): p. 196-209.
746 46. Benassi, M.S., et al., *Alteration of pRb/p16/cdk4 regulation in human osteosarcoma.* Int J Cancer,
747 1999. **84**(5): p. 489-93.
748 47. Maitra, A., et al., *Loss of p16(INK4a) expression correlates with decreased survival in pediatric*
749 *osteosarcomas.* Int J Cancer, 2001. **95**(1): p. 34-8.
750 48. Benavente, C.A. and M.A. Dyer, *Genetics and epigenetics of human retinoblastoma.* Annu Rev
751 Pathol, 2015. **10**: p. 547-62.
752 49. Wu, S.C. and C.A. Benavente, *Chromatin remodeling protein HELLS is upregulated by inactivation*
753 *of the RB-E2F pathway and is nonessential for osteosarcoma tumorigenesis.* Oncotarget, 2018.
754 **9**(66): p. 32580-32592.
755 50. Rane, S.G., et al., *Germ line transmission of the Cdk4(R24C) mutation facilitates tumorigenesis*
756 *and escape from cellular senescence.* Mol Cell Biol, 2002. **22**(2): p. 644-56.
757 51. Nuovo, G.J., et al., *In situ detection of the hypermethylation-induced inactivation of the p16 gene*
758 *as an early event in oncogenesis.* Proc Natl Acad Sci U S A, 1999. **96**(22): p. 12754-9.
759 52. Fry, D.W., et al., *Specific inhibition of cyclin-dependent kinase 4/6 by PD 0332991 and associated*
760 *antitumor activity in human tumor xenografts.* Mol Cancer Ther, 2004. **3**(11): p. 1427-38.
761 53. Endo-Munoz, L., et al., *Progression of Osteosarcoma from a Non-Metastatic to a Metastatic*
762 *Phenotype Is Causally Associated with Activation of an Autocrine and Paracrine uPA Axis.* PLoS
763 One, 2015. **10**(8): p. e0133592.
764 54. Vassalli, J.D. and D. Belin, *Amiloride selectively inhibits the urokinase-type plasminogen activator.*
765 FEBS Lett, 1987. **214**(1): p. 187-91.
766 55. Jeanblanc, M., et al., *The retinoblastoma gene and its product are targeted by ICBP90: a key*
767 *mechanism in the G1/S transition during the cell cycle.* Oncogene, 2005. **24**(49): p. 7337-7345.
768 56. Dyson, N.J., *RB1: a prototype tumor suppressor and an enigma.* Genes Dev, 2016. **30**(13): p.
769 1492-502.
770 57. Madan, B., et al., *Bone loss from Wnt inhibition mitigated by concurrent alendronate therapy.*
771 Bone Res, 2018. **6**: p. 17.

772

773

Wu et al
Figure 1

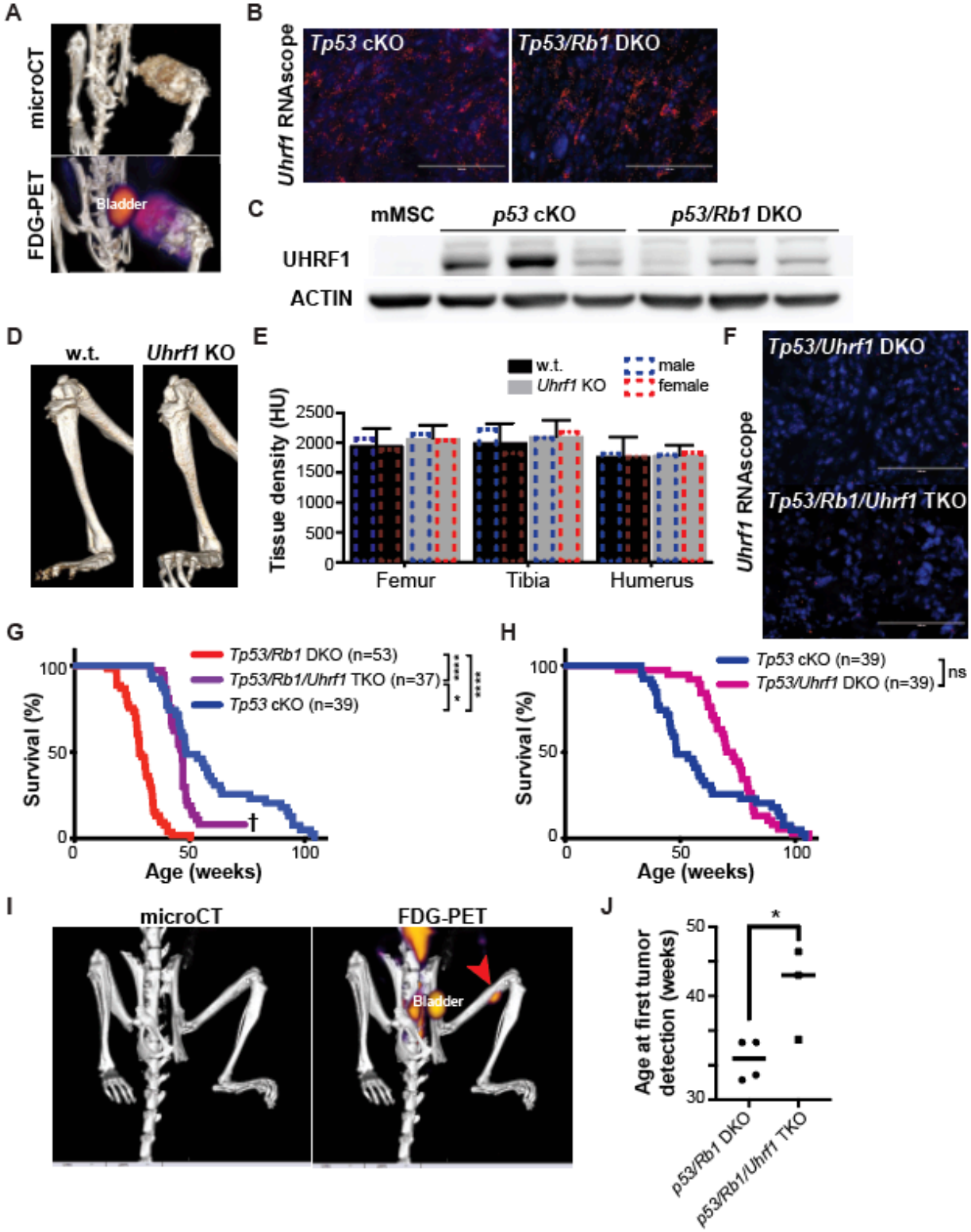

774

775 **Figure 1. UHRF1 is a critical driver of the increased malignancy observed in *Rb1* null osteosarcoma**

776 (A) Representative micro-CT (top) and micro-PET (bottom) scans of OS that arises in a mouse femur. (B)
777 Representative fluorescent images of *in situ* hybridizations using RNAscope on tumors from genetically
778 engineered OS mice using a probe against *Uhrf1* (red). Nuclei were counterstained with DAPI (blue).
779 *Uhrf1* expression is detected in *Tp53* cKO and *Tp53/Rb1* DKO mice. (C) Western blot detection of UHRF1
780 in tumors from genetically engineered *p53* cKO and *p53/Rb1* DKO OS mice, β-actin was used as loading
781 control. (D) Micro-CT scan of hind limb from wildtype (w.t.) and preosteoblastic *Uhrf1* knockout (*Uhrf1*
782 KO) mice (E) Bone density analysis of prime OS locations in Hounsfield units (HU). Each data point is
783 mean ± s.d. of n=4 samples. (F) Representative fluorescent images of *in situ* hybridizations using
784 RNAscope on tumors from genetically engineered OS mice using a probe against *Uhrf1* (red). Nuclei
785 were counterstained with DAPI (blue). *Uhrf1* expression is not detected in *Tp53/Uhrf1* DKO and
786 *Tp53/Rb1/Uhrf1* TKO mice. (G-H) Kaplan-Meier curves showing the survival of osteosarcoma-prone
787 mouse models. (G) Mice bearing *Rb1* mutations *Tp53/Rb1* DKO: *Osx-Cre; p53*$^{lox/lox}$*; Rb1*$^{lox/lox}$ (red; n=53)
788 have significantly shorter lifespan compared to *Tp53* cKO: *Osx-Cre; p53*$^{lox/lox}$*; Rb1*$^{lox/lox}$ (blue; n=39). This
789 survival time was significantly increased in *Tp53*/*Rb1*/*Uhrf1* TKO: *Osx-Cre; p53*$^{lox/lox}$*; Rb1*$^{lox/lox}$*;Uhrf1*$^{lox/lox}$
790 (purple; n=37) mice. † Three surviving mice were removed from study to confirm tumor absence. (H)
791 *Tp53*/*Uhrf1* DKO: *Osx-Cre; p53*$^{lox/lox}$*; Uhrf1*$^{lox/lox}$ (magenta; n=39) showed an overall survival comparable
792 to *Tp53* cKO (blue; n=39). Mantel-Cox test were used for curve comparisons. ns=not significant, * $p <$
793 0.05, **** $p < 0.0001$. (I) Representative images from micro-CT (left) and micro-PET (right) scans used
794 for determining the age at which tumors can be first detected (red arrow). (J) Age of mice (in weeks) at
795 earliest tumor detection via micro-CT and PET scans. Solid line represents the average for *Tp53/Rb1* DKO
796 (n=4) and *Tp53*/*Rb1*/*Uhrf1* TKO (n=3). *$p < 0.05$ by unpaired two-tailed *t* test.

797

Wu et al
Figure 2

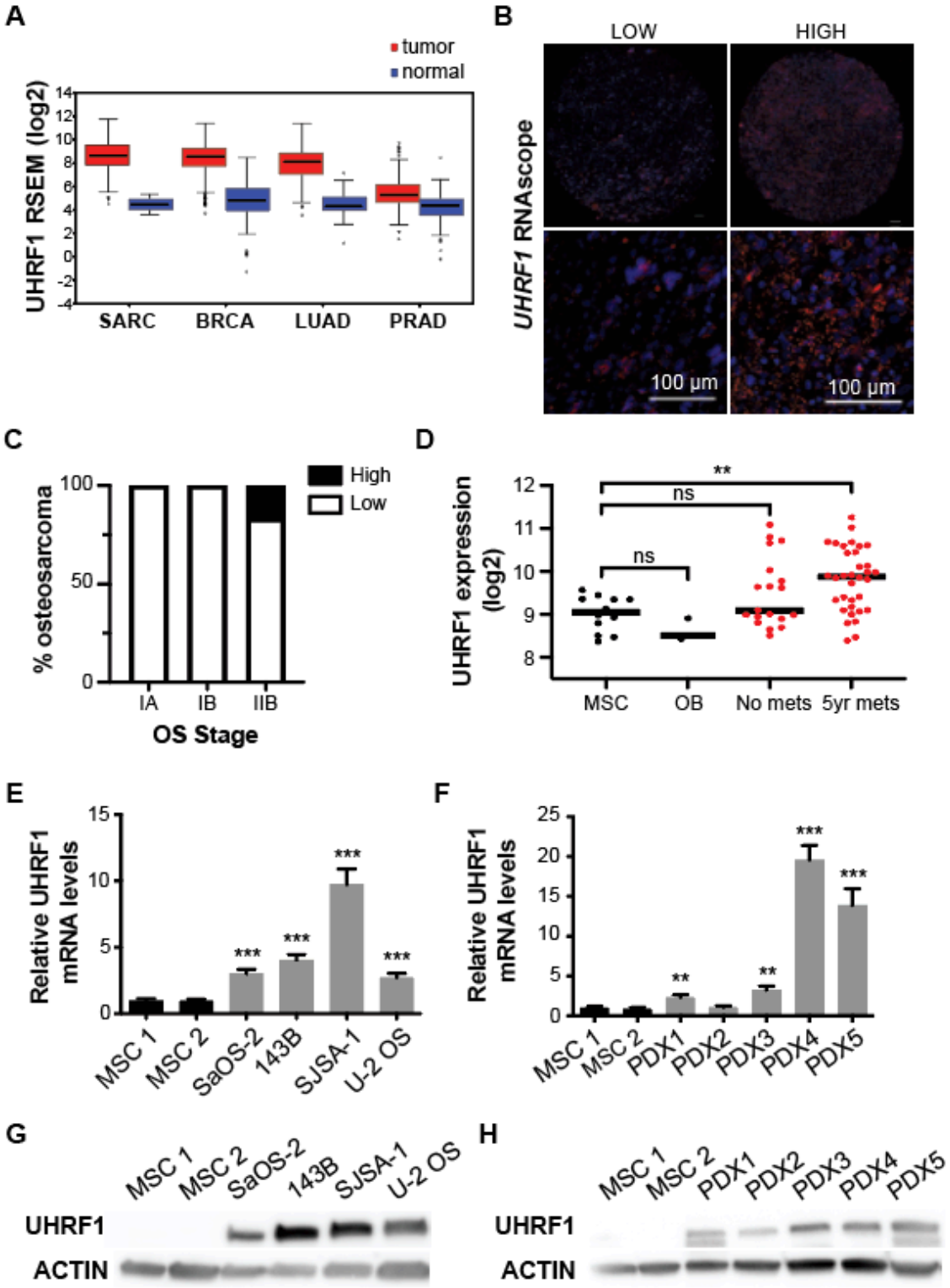

798

799 **Figure 2. UHRF1 is upregulated and overexpressed in human osteosarcoma**

800 (A) The Cancer Genome Atlas data of RNA-Seq by expectation-maximization (RSEM) values from 263
801 human sarcoma (SARC) tumor samples compared to 2 normal tissue (17.9-fold), 1100 breast invasive
802 carcinoma (BRCA) compared to 112 normal (13.5-fold), 517 lung adenocarcinoma (LUAD) compared to
803 59 normal (13.7-fold) showing increased *UHRF1* expression in tumors with frequent RB pathway
804 alterations but not in 498 prostate adenocarcinoma (PRAD) tumors compared 52 normal (1.84-fold)
805 were RB pathway is normally unaltered. Tumor samples depicted in red compared to normal samples in
806 blue. (B) Representative fluorescent images in 2X (top) and 20X (bottom) magnification of *in situ*
807 hybridizations using RNAscope scored as low or high based on signal intensity for *UHRF1* mRNA. Scale
808 bar = 100 µm. (C) Quantification of the percentage of low and high signal score acquired from RNAscope
809 in stage IA, IB, and IIB OS. (D) RNA-seq analysis comparing *UHRF1* expression between mesenchymal
810 stem cells (MSC), osteoblasts (OB), and high-grade OS biopsies from patients who did (5yr mets) or did
811 not develop metastasis (No mets) within 5 years from diagnoses showing increased *UHRF1* expression in
812 metastasis-prone tumors. (E-F) qPCR analysis of *UHRF1* mRNA in (E) human OS cell lines (143B, SJSA-1,
813 SaOS-2 and U-2 OS) and (F) patient-derived xenografts (PDX1-5). All data are mean ± SD normalized to
814 MSC (n=3). (G-H) Western blot detection of UHRF1 in (G) human OS cell lines, and (H) PDXs tumors, β-
815 actin was used as loading control. ** $p < 0.01$, *** $p < 0.001$ by unpaired two-tailed *t* test.

816

Wu et al
Figure 3

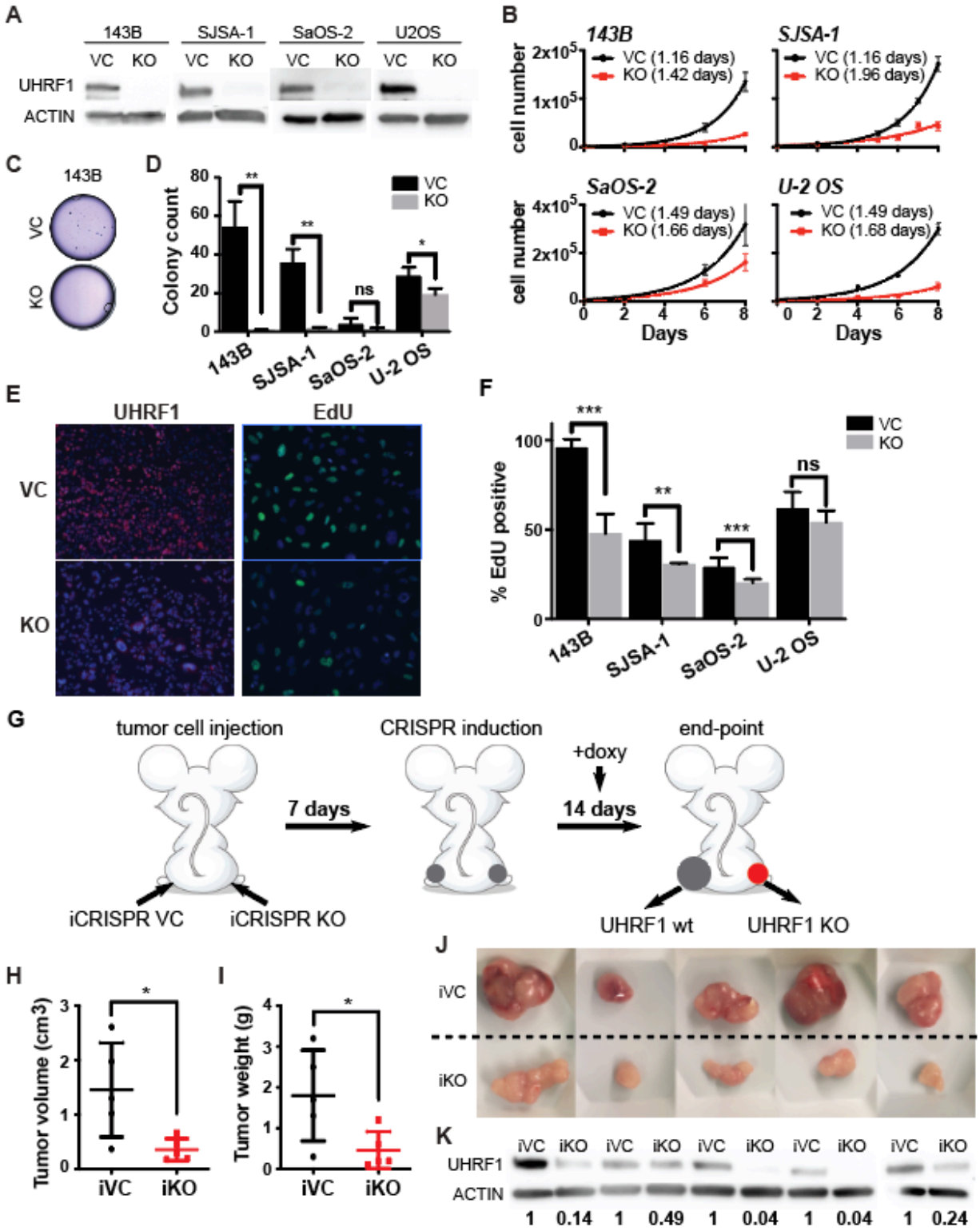

817

818 **Figure 3. UHRF1 promotes human OS tumor growth *in vitro* and *in vivo***

819 (A) Western blot verification of CRISPR/Cas9-mediated UHRF1 knockout of human OS cell lines (KO) in
820 comparison to non-targeting vector control (VC). β-actin was used as loading control. (B) Growth curves
821 of UHRF1 knockout cells (KO, red) compared to control (VC, black), population doubling time indicated in
822 parentheses. (C) Representative images from clonogenic assay plates with 143B VC and UHRF1 KO. (D)
823 Histogram of colony counts from clonogenic assay. ns=not significant; * $p < 0.05$, ** $p < 0.01$ by unpaired
824 two-tailed *t* test. (E) Representative images of cells labelled with Click-iT EdU (green) or immunostained
825 with UHRF1 (red). Nuclei were counterstained with DAPI (blue). (F) Quantification of EdU signal from
826 immunocytochemistry probing UHRF1 and EdU in VC and UHRF1 KO human OS cell lines. ns=not
827 significant; ** $p < 0.01$, *** $p < 0.001$ by unpaired two-tailed *t* test. (G) Cartoon representation for
828 doxycycline-inducible *in vivo* knockout for flank-injected osteosarcoma cell lines carrying a non-targeting
829 sgRNA (iCRISPR VC) or UHRF1 sgRNA (iCRISPR KO). (H-I) Quantification of the tumor (H) volume and (I)
830 weight for each of the replicates. * $p<0.05$ by paired two-tailed *t* test. (J) Images from tumors collected
831 from subcutaneous injection of iCRISPR VC (iVC, n=5) and iCRISPR KO (iKO, n=5) SJSA-1. (K) Western blot
832 verification of UHRF1 knockout in iKO compared to iVC for tumors shown in J. β-actin was used as
833 loading control. UHRF1 densitometry quantification normalized to the matching iVC, prior normalization
834 to β-actin.

835

Wu et al
Figure 4

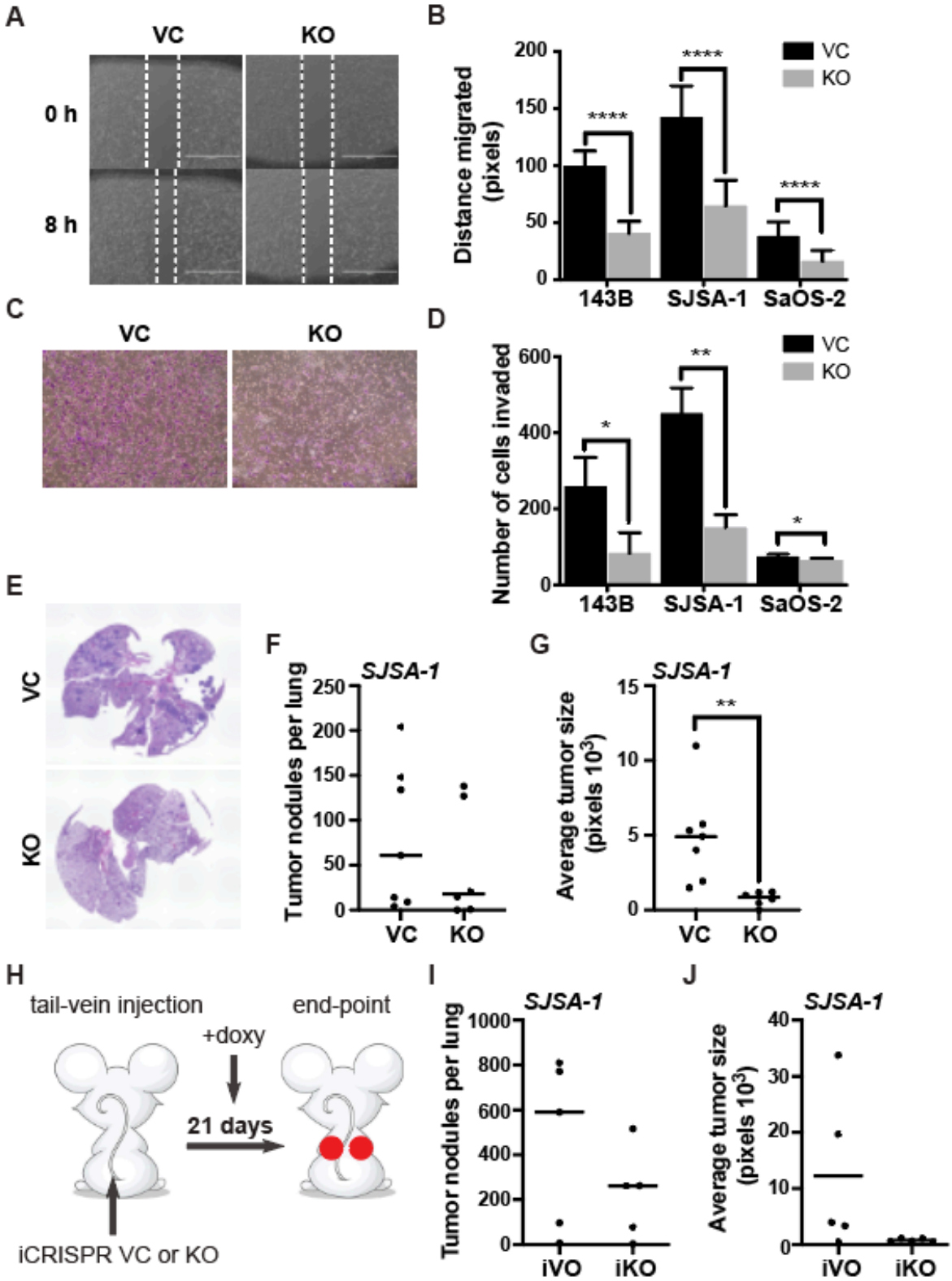

836

837 **Figure 4. UHRF1 promotes human OS cell migration and invasion *in vitro* and *in vivo***

838 (A) Representative image from scratch-wound assay comparing wound closure of non-targeting vector
839 control (VC) and UHRF1 KO (KO) cells over 8 h in SJSA-1 cells. White dashed lines represent wound edge.
840 (B) Quantification of distance (pixels) migrated in scratch-wound assays for each of the osteosarcoma
841 cell lines. Each data point is mean ± s.d. of ten measurements in triplicate samples. (C) Representative
842 images from Transwell assays with cells stained with crystal violet (purple) comparing levels of invasion
843 between VC and UHRF1 KO in SJSA-1 cells. (D) Quantification of number of cells invaded across the
844 Transwell membrane for each of the osteosarcoma cell lines. Each data point is mean ± s.d. of triplicate
845 samples. (E) Representative H&E staining from lung sections collected from mice injected intravenously
846 with VC or UHRF1 KO SJSA-1 cells. Pulmonary nodules were quantified by (F) the number of tumor
847 nodules found per lung and by (G) the average tumor size per lung. Solid line represents the average
848 from n=7 for VC and n=6 for KO. (H) Cartoon representation for doxycycline-inducible *in vivo* knockout
849 for tail-vein-injected osteosarcoma cell lines carrying a non-targeting sgRNA (iCRISPR VC; iVC) or UHRF1
850 sgRNA (iCRISPR KO; iKO) to assess lung metastases. (I-J) Pulmonary nodules were quantified by (I) the
851 number of tumor nodules found per lung and by (J) the average tumor size per lung. Solid line
852 represents the average from five replicates for each condition. For all graphs: ** $p < 0.01$, *** $p < 0.001$,
853 **** $p < 0.0001$ by unpaired two-tailed *t* test.

Wu et al
Figure 5

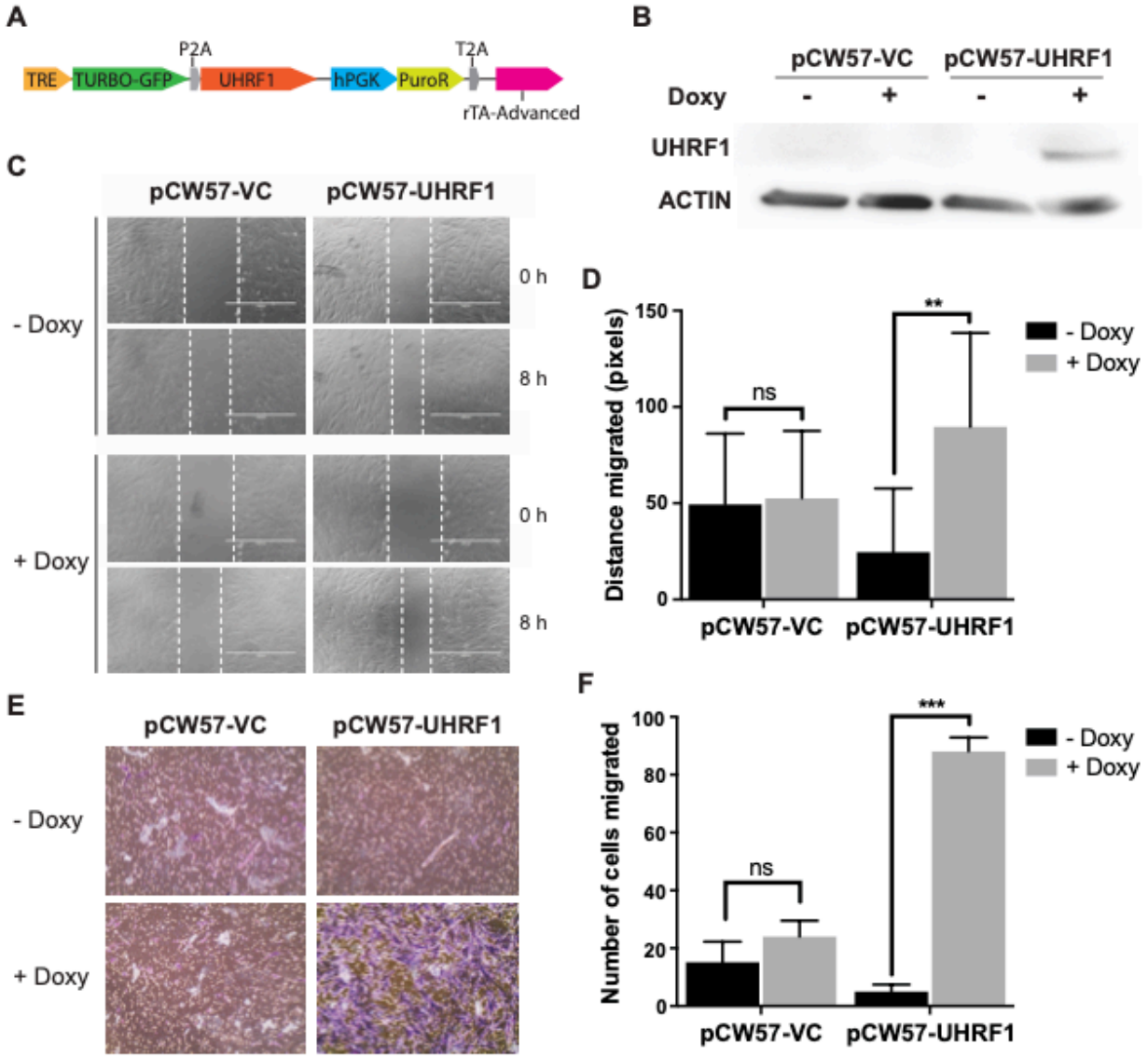

854

855 **Figure 5. UHRF1 overexpression promotes human MSC cell migration and invasion**

856 (A) Plasmid map of the doxycycline inducible UHRF1 overexpression system. Tet Response Element (TRE)
857 is activated by doxycycline binding to the reverse tetracycline-controlled transactivator (rTA), allowing
858 transcription of GFP and the pCW57-promoter driven human UHRF1 cDNA. (B) Western blot detection
859 of UHRF1 in MSCs transduced with vector control (pCW57-VC) or UHRF1 overexpression (pCW57-UHRF1)
860 plasmid, treated with DMSO (-) or doxycycline (+). (C) Scratch-wound assay in MSC culture comparing

861 wound closure of control (pCW57-VC) and UHRF1 overexpressed (pCW57-UHRF1) cells over 8 h span.
862 White dashed lines represent wound edge. (D) Histogram quantification of distance (pixels) migrated for
863 doxycycline non-induced (black) and induced (gray) pCW57-VC and pCW57-UHRF1. Each data point is
864 mean ± s.d. of ten measurements in triplicate samples. (E) Representative images from Transwell assays
865 with cells stained with crystal violet comparing levels of invasion between doxycycline non-induced and
866 induced pCW57-VC and pCW57-UHRF1 MSC. (F) Quantification of the number of cells invaded across the
867 Transwell membrane. Each data point is mean ± s.d. of triplicate samples. For all graphs: ns=not
868 significant, ** $p < 0.01$, *** $p < 0.001$, by unpaired two-tailed *t* test.

Wu et al
Figure 6

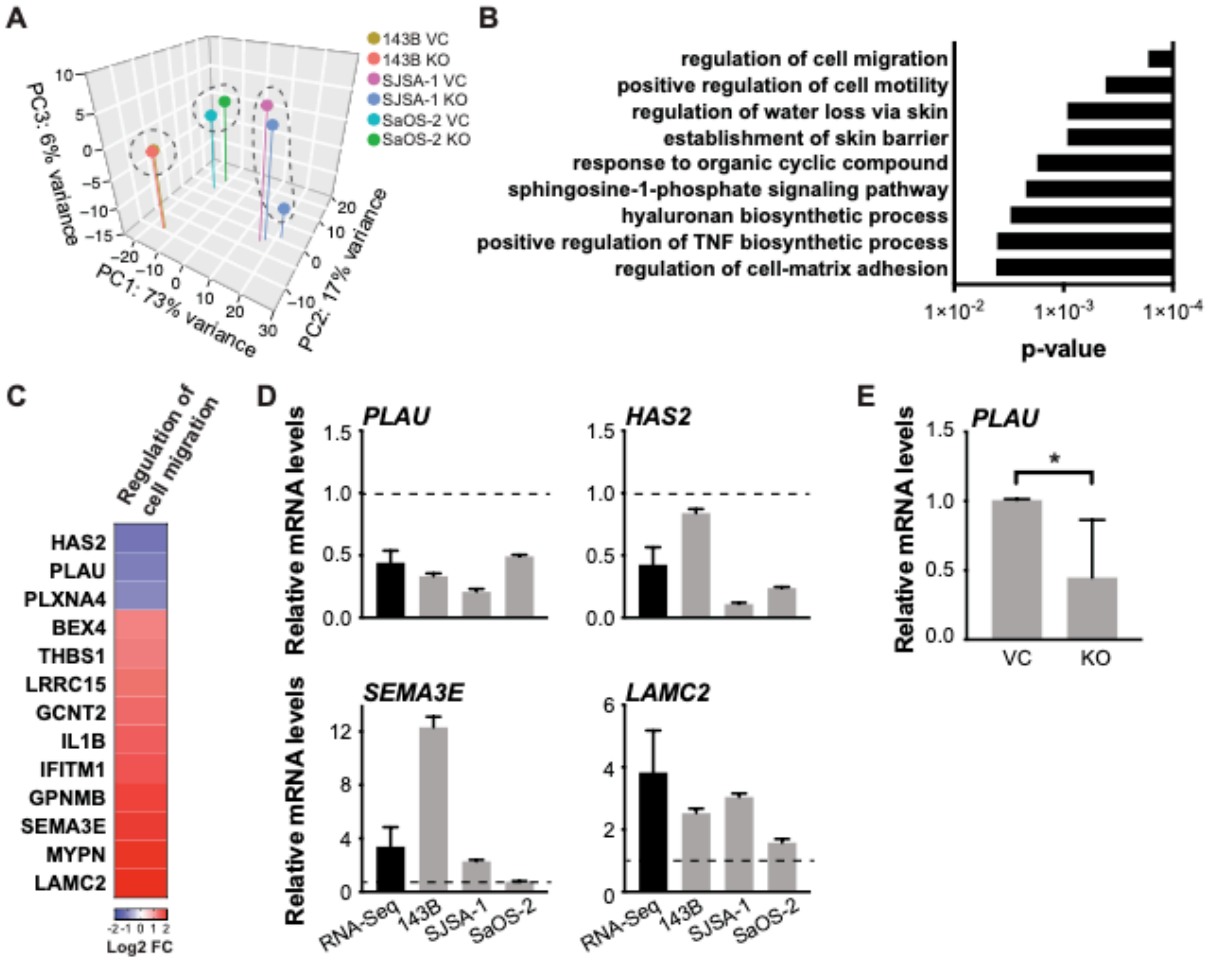

Figure 6. UHRF1 controls the expression of genes involved in cell migration and invasion

(A) Principle component analysis (PCA) plot generated from RNA-seq displaying gene expression profile in VC and KO OS cells. (B) Gene ontology (GO) analysis for biological process of differentially expressed genes (DEGs) identified through RNA-seq. (C) Heat map of top 13 genes involved in regulation of cell migration, decreased (blue) or increased (red) in expression level upon UHRF1 loss. (D) qPCR analysis confirming expression changes of migration related genes in individual cell lines upon UHRF1 loss, fold change of mRNA level normalized to vector control (gray), compared with average fold change from RNA-seq analysis (black). (E) qPCR analysis of *PLAU* mRNA levels in flank-implanted tumors from control (VC) and UHRF1 KO (KO) SJSA-1 cell lines. * $p<0.05$ by paired two-tailed *t* test.

Wu et al
Figure 7

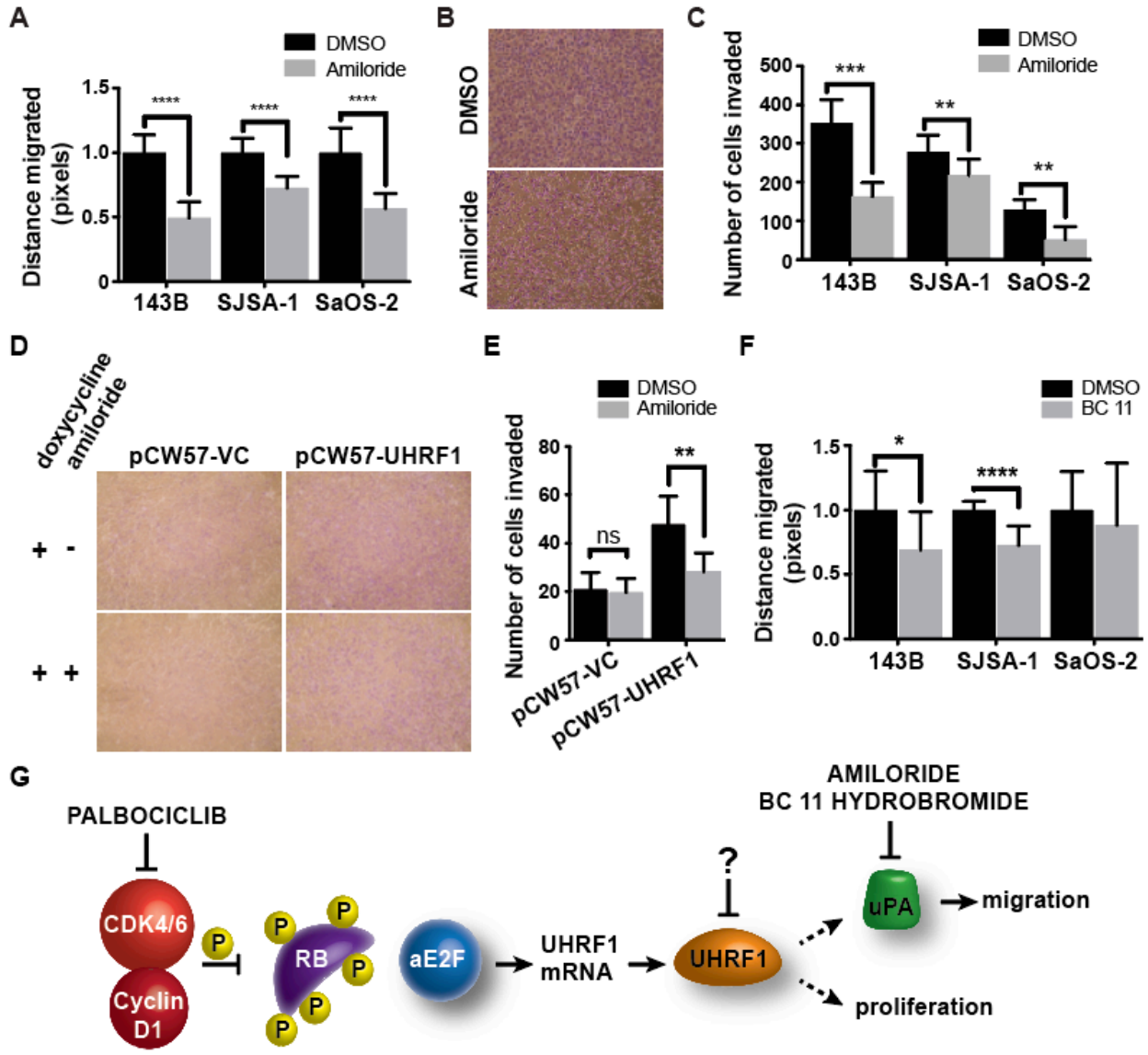

Figure 7. Urokinase plasminogen activator contributes to osteosarcoma migration

(A) Quantification of distance (pixels) migrated in scratch-wound assays for each of the osteosarcoma cell lines treated with DMSO or 150 µM amiloride in SJSA-1, normalized to DMSO control. Each data point is mean ± s.d. of ten measurements in triplicate samples. (B) Representative images from Transwell assays with cells stained with crystal violet comparing levels of invasion between cells treated with DMSO or 150 µM amiloride in SJSA-1. (C) Quantification of the number of cells invaded in Transwell

886 invasion assay for each of the osteosarcoma cell lines treated with DMSO or 150 µM amiloride. Each
887 data point is mean ± s.d. of triplicate samples. (D) Representative images from Transwell assays with
888 cells stained with crystal violet comparing levels of invasion between doxycycline induced pCW57-VC
889 and pCW57-UHRF1 MSC treated with DMSO or 150 µM amiloride. (E) Quantification of the number of
890 MSC invaded across the Transwell membrane from experiment shown in D. Each data point is mean ±
891 s.d. of triplicate samples. (F) Quantification of distance (pixels) migrated in scratch-wound assays for
892 each of the osteosarcoma cell lines treated with DMSO or 16.4 µM BC 11 hydrobromide in SJSA-1,
893 normalized to DMSO control. Each data point is mean ± s.d. of ten measurements in triplicate samples.
894 For all graphs: ns=not significant, ** $p < 0.01$, *** $p < 0.001$, by unpaired two-tailed *t* test. (G) Model of
895 UHRF1 oncogenic function in osteosarcoma. In the absence of RB or upon RB inactivation via
896 hyperphosphorylation, activator E2Fs drive *UHRF1* transcription. The resulting UHRF1 protein
897 overexpression stimulates proliferation and uPA overexpression, aiding to migration, invasion, and
898 metastasis. For osteosarcomas with CDK4/6 amplification, palbociclib treatment is an effective way to
899 reduce UHRF1 expression and result in decreased proliferation and migration. Downstream of UHRF1,
900 uPA inhibitors (e.g. amiloride, BC 11 hydrobromide) are attractive therapeutic options to decrease
901 migration and metastasis. For most osteosarcomas (with or without *RB1* mutations), the development
902 of UHRF1-targeted therapeutics might result in beneficial decrease in both tumor growth and
903 pulmonary metastases.